Journal of Sound and Vibration (1999) **220**(4), 695–727
Article No. jsvi.1998.1953, available online at http://www.idealibrary.com on IDEAL

AN ASYMPTOTIC-NUMERICAL METHOD FOR LARGE-AMPLITUDE FREE VIBRATIONS OF THIN ELASTIC PLATES

L. AZRAR

Laboratoire des Systèmes Dynamiques, Théorie, Applications et Synthèses, Département de Mathématiques, Faculté des Sciences et Techniques de Tanger, Université Abdelmalek Essaadi, BP 416 *Tanger, Morocco*

R. BENAMAR

Laboratoire d'Études et de Recherches en Simulation, Instrumentation et Mesures, E.G.T., École Mohammadia d'Ingénieurs, Université Mohammed V, BP 765 *Agdal, Rabat, Morocco*

AND

M. POTIER-FERRY

Laboratoire de Physique et Mécanique des Matériaux, U.R.A. CNRS 1215, *I.S.G.M.P. Université de Metz, Ile du Saulcy*, 57045 *Metz Cedex, France*

(*Received* 2 *February* 1998, *and in final form* 14 *September* 1998)

An Asymptotic-Numerical Method has been developed for large amplitude free vibrations of thin elastic plates. It is based on the perturbation method and the finite element method. This method eliminates the major difficulties of the classical perturbation methods, namely the complexity of the right hand sides and the limitation of the validity of the solution obtained. The applicability of this method to non-linear vibrations of plates is clearly presented. Based on the Von Karman theory and the harmonic balance method, a cubic non-linear operational formulation has been obtained. By using the mixed stress–displacement Hellinger–Reissner principle, a quadratic formulation is given. The displacement and frequency are expanded into power series with respect to a control parameter. The non-linear governing equation is then transformed into a sequence of linear problems having the same stiffness matrix, which can be solved by a classical FEM. Needing one matrix inversion, a large number of terms of the series can be easily computed with a small computation time. The non-linear mode and frequency are then obtained up to the radius of convergence. Taking the starting point in the zone of validity, the method is reapplied in order to determine a further part of the non-linear solution. Iteration of this method leads to a powerful incremental method. In order to increase the validity of the perturbed solution, another technique, called Padé approximants, is shrewdly incorporated. The solutions obtained by these two concepts coincide perfectly in a very large part of the backbone curve. Comprehensive numerical tests for non-linear free vibrations of circular, square, rectangular and annular plates with various boundary conditions are reported and discussed.

0022–460X/99/090695 + 33 $30.00/0

1. INTRODUCTION

The modal analysis and linearising techniques are routinely used to examine the dynamic response of structures. However, standard procedures are based on the assumption of linearity and can fail to give accurate results when the amplitude of vibration is large enough to induce significant non-linear behaviour. The study of large amplitude vibrations of plates involving geometrical non-linearities requires efficient non-linear procedures. Previous investigations on the non-linear vibrations of plates have used analytical or numerical methods. The analytical methods are based on the assumption of the known functions satisfying boundary conditions. However, this is limited to simple boundary conditions and standard shapes of the plate, and the in-plane equilibrium is not generally satisfied. The numerical methods based on the finite element method, generally encountered in practice in computing codes, are based on the modal analysis techniques. This is very useful, but limited to small amplitudes ($w/h \ll 1$). For large amplitudes, numerical procedures for non-linear problems are necessary. Some solution algorithms for non-linear problems are implemented in different codes but they are very time consuming and are not easy to manipulate. The significant advantage of the method proposed here is the combination of the finite element method and the perturbation method providing an efficient algorithm for solving the obtained non-linear problem. This procedure is not computationally more expensive than the standard modal analysis.

For a survey of the literature on non-linear vibrations of plates, the most commonly used methods are presented. The assumption generally used is the separation of time and space variables. The first approach is based on the assumption that the non-linear mode shape is the same as the linear one. Using Galerkin's method, one can reduce the governing dynamic equations to a single non-linear ordinary differential equation in time of Duffing type. The latter equation is treated by elliptical functions or by a harmonic balance method [1–5]. A numerical resolution and a direct numerical integration method are also used [6–8]. The assumption of the displacement in the form of double a Fourier series leads to a non-linear algebraic system which can be solved by an incremental-iterative method [9]. A comprehensive survey of the large amplitude vibrations of plates has been presented in references [10–11]. In the second approach, the dependence on time is assumed to be harmonic. Then, one can use the harmonic balance method to obtain a non-linear boundary value problem in the spatial variable. This technique is widely used because it permits one to transform the non-linear dynamic problem into a non-linear static one. This allows one to work with the same numerical methods as in static. Using the linearized strain–displacement relations, the frequency–amplitude relations have been obtained applying the Rayleigh–Ritz method [12]. The classical finite element method can be used for an accurate solution of complex engineering problems. The first attempt to apply the later method in large amplitude vibration is due to Mei [13]. Most studies in non-linear vibrations of structures using this approach have been carried out by combining the finite element method and linearising procedures [13–18]. As clearly presented in references [14, 17, 18], this procedure leads to an iterative linear eigenvalue problem. It is well known that the

discretisation of the structure leads to a large scale problem. Then, on the one hand, the iterative procedure at each point of the solution is very time consuming. On the other hand, this formulation reduces the effect of the non-linearity [19]. Without linearising functions, the problem of non-linear free vibration is represented as a non-linear eigenvalue problem which can be solved by an incremental-iterative procedure [20]. An amplitude-incremental plate element is presented and applied to study the periodic vibration of thin plates in reference [21]. Different authors used the reduced basis technique or the Ritz method [22, 23]. These papers demonstrated the effectiveness of reduction methods in non-linear vibrations of beams and plates. The dynamic behaviour of plates at large vibration amplitudes was examined both theoretically using a multi-mode analysis, and experimentally by White *et al*. and by Benamar *et al*. [24–27]. Following the same procedure, a semi-analytical approach has been proposed for forced vibrations. This leads to non-linear algebraic equations which can be solved by an incremental-iterative procedure. The application of this method to the forced non-linear vibrations of beams has been recently developed [28, 29].

In the third approach one determines an approximate solution of non-linear dynamic problems by treating the continuous problem directly without the above mentioned simplifying assumptions. Various methodological approaches can be used like, for example, the method of multiple scales. For a comprehensive review of the literature, we refer the reader to Nayfeh *et al*.'s works [30–32]. Other methods like incremental time space finite strip or alternating frequency–time domain can be used [33, 34]. The complete time-space problem has to be solved without any simplification. Remembering the difficulties in solving numerically some static or stationary problems, one understands that such methods will not be workable in practice for a long time. Thus, it is relevant to look for simpler techniques for solving time-dependent problems.

The harmonic balance method is a well known application for highly non-linear systems and is largely used for non-linear vibrations of elastic structures. Using this approach, one gets a non-linear differential problem that is similar to a static one. The resolution of this problem permits one to obtain the non-linear modes of vibration and the backbone curves which are simple dynamic characteristics of the system. In general, the computational methods used to solve this problem are the incremental iterative methods. The most popular one is a Newton–Raphson method associated with control parameters. The principle is to follow the non-linear solution path in a stepwise manner, via a sequence of linearizations and some iterations to achieve equilibrium. With a proper parametrisation of the branch, such algorithms are successful in determining a complete shape of solution that will be represented point by point. However, this requires a long computation time compared to a linear problem and it is difficult to automatize as for step by step procedures. An alternative approach corresponds to analytical representation techniques such as the perturbation methods. According to these representation techniques, the solution of the whole problem is represented in the form of power series with respect to a path parameter. The principle of these methods is to determine some terms of the series by solving a recursive set

of linear problems. In contrast with the incremental-iterative methods, perturbation methods have received much less attention from the computational community. There are two main explanations for the poor success of such methods in computational context. The first one is the growing complexity of the right-hand sides of the linear problems obtained. The second is the thought that the analytical representation is valid only for very small values of the perturbation parameter. So, these methods are usually considered more as a theoretical framework for qualitative analysis than as a numerical tool to furnish accurate qualitative results.

An Asymptotic-Numerical Method based on perturbation techniques and the finite element method has been developed for non-linear problems. This method permits one to remove some of the previous difficulties in the classical perturbation methods. It has been used by Damil and Potier-Ferry [35] for computing perturbed bifurcation and applied by Azrar *et al*. [36–39] for computing the post-buckling behaviour of elastic plates and shells. Next, it has been extended to some non-linear elastostatic problems by Cochelin *et al*. [40, 41]. An application of this method to non-linear vibrations is presented by Azrar *et al*. [42]. These works have brought out the essential features that affect the practicability of *the coupling of perturbation methods and finite element methods*. The principle of this method is to represent the unknowns (displacements, load parameters, frequency, . . .) by a power series expansion with respect to a control parameter. By introducing the expansion into the governing equation, the non-linear problem is transformed into a sequence of simple linear problems which can be solved by a classical finite element method. Hence, a large number of terms of the series can be numerically computed.

The main objective of this paper is to present the development of the asymptotic numerical method for large amplitude vibrations of plates. The paper is organised as follows. First, the governing equations based on the von-Karman's plate theory are presented. The use of the harmonic balance method permits one to obtain a simple operational formulation. The asymptotic numerical method based on the finite element method has been developed and applied for solution. Comprehensive numerical tests for non-linear free vibrations of plates are reported and discussed. However, the validity of the solution obtained is limited. Taking the starting point in the zone of validity and reapplying the ANM, a path following procedure is obtained. This continuation method leads to a very powerful incremental method with an analytical step. The limitation of the validity of the solution has been overcome and the whole backbone curve is analytically obtained in a few steps. The orthogonalisation of the basis vectors and the rearrangement of the computed series has been presented in order to extract the maximum information. The resulting coefficients are approximated by Padé approximants. A short computation time is needed for these manipulations. A good choice of these approximants leads to a considerable improvement in the zone of validity. The solutions obtained by the continuation procedure and Padé approximants coincide perfectly in a very large part of the backbone curve. The large amplitude free vibrations of circular, square, rectangular and annular plates with various boundary conditions are presented and discussed.

2. MATHEMATICAL FORMULATION

The non-linear differential equations governing the moderately large amplitude vibration of thin elastic plates can be obtained from von Karman's deflection theory of plates. The displacement variational principle of these equations leads to a cubic non-linearity. The mixed stress–displacement approach, called the Hellinger–Reissner principle, leads to an only quadratic non-linearity. Then in view of applying the expansion procedure, the mixed approach is preferred here since it leads to simple algebra. After the expansion process, a displacement formulation will be used, namely the very classical displacement finite element method.

2.1. STRAIN AND KINETIC ENERGY

Denote the displacement of the middle surface of the plate by u, v and w, where u and v are the in-plane displacements and w the transverse displacement in the x, y and z directions, respectively. The reference plane $z = 0$ may be chosen at an arbitrary location through the undeformed plate and the z-axis directed normally to it. For thin structures, the Green–Lagrange strains are supposed to vary linearly through the thickness z and are given by

$$\boldsymbol{\Gamma}(u, v, w) + z\boldsymbol{\kappa}(u, v, w), \tag{1}$$

with $\boldsymbol{\Gamma}(u, v, w) = \boldsymbol{\Gamma}^L(u, v, w) + \boldsymbol{\Gamma}^{NL}(u, v, w)$. The tensors $\boldsymbol{\Gamma}$ and $\boldsymbol{\kappa}$ are the generalised membrane strains and bending strains. The membrane strains $\boldsymbol{\Gamma}$ are separated into a linear part $\boldsymbol{\Gamma}^L$ and non-linear part $\boldsymbol{\Gamma}^{NL}$, ($\boldsymbol{\Gamma} = \boldsymbol{\Gamma}^L + \boldsymbol{\Gamma}^{NL}$). From the von Karman deflection theory of plates [11], the components of these generalised strain tensors are defined as:

$$\boldsymbol{\Gamma}^L = \begin{Bmatrix} \dfrac{\partial u}{\partial x} \\ \dfrac{\partial v}{\partial y} \\ \dfrac{\partial u}{\partial y} + \dfrac{\partial v}{\partial x} \end{Bmatrix}, \qquad \boldsymbol{\Gamma}^{NL} = \begin{Bmatrix} \dfrac{1}{2}\left(\dfrac{\partial w}{\partial x}\right)^2 \\ \dfrac{1}{2}\left(\dfrac{\partial w}{\partial y}\right)^2 \\ \dfrac{\partial w}{\partial x}\dfrac{\partial w}{\partial y} \end{Bmatrix}; \qquad \boldsymbol{\kappa} = \begin{Bmatrix} -\dfrac{\partial^2 w}{\partial x^2} \\ -\dfrac{\partial^2 w}{\partial y^2} \\ -2\dfrac{\partial^2 w}{\partial x\,\partial y} \end{Bmatrix}. \tag{2}$$

The bending strain $\boldsymbol{\kappa}$ is supposed to be linear with respect to the displacement (framework of moderate rotations). The membrane or in-plane forces $\mathbf{N}$ and moments $\mathbf{M}$ are assumed to be related to the strain and curvature by the constitutive relations:

$$\mathbf{N} = \begin{Bmatrix} N_x \\ N_y \\ N_{xy} \end{Bmatrix} = [\mathbf{C}_m]{:}\boldsymbol{\Gamma}; \qquad \mathbf{M} = \begin{Bmatrix} M_x \\ M_y \\ M_{xy} \end{Bmatrix} = [\mathbf{C}_b]{:}\boldsymbol{\kappa}, \tag{3a}$$

in which $\mathbf{C}_m$ and $\mathbf{C}_b$ are symmetric matrices of material properties. For isotropic plates of uniform thickness h, (E: Young's modulus, v: Poisson's ratio).

$$\mathbf{C}_m = \frac{Eh}{1-v^2}\begin{bmatrix} 1 & v & 0 \\ v & 1 & 0 \\ 0 & 0 & \dfrac{1-v}{2} \end{bmatrix} \qquad \mathbf{C}_b = \frac{Eh^3}{12(1-v)^2}\begin{bmatrix} 1 & v & 0 \\ v & 1 & 0 \\ 0 & 0 & \dfrac{1-v}{2} \end{bmatrix}. \tag{3b}$$

The total strain energy expression of the plate can be written as:

$$P(u, v, w) = \frac{1}{2}\int_\Omega (\boldsymbol{\Gamma}\colon \mathbf{C}_m \colon \boldsymbol{\Gamma} + \boldsymbol{\kappa}\colon \mathbf{C}_b \colon \boldsymbol{\kappa})\, \mathrm{d}\Omega. \tag{4}$$

Since $\boldsymbol{\Gamma}$ is quadratic in (u, v, w), $P(u, v, w)$ is of the degree 4 with respect to (u, v, w). To reduce the order of the non-linearity, an additional variable is introduced. This can be achieved by using the mixed Hellinger–Reissner functional:

$$H(u, v, w, \mathbf{N}) = \int_\Omega (\mathbf{N}\colon \boldsymbol{\Gamma} - \tfrac{1}{2}\,\mathbf{N}\colon \mathbf{C}_m^{-1} : \mathbf{N} + \tfrac{1}{2}\,\boldsymbol{\kappa}\colon \mathbf{C}_b \colon \boldsymbol{\kappa})\, \mathrm{d}\Omega \tag{5a}$$

where the unknown is the mixed (displacement-stress) vector field

$$\mathbf{U} = {}^t[u, v, w, \mathbf{N}] \tag{5b}$$

The mixed functional H is cubic in $(u, v, w, \mathbf{N})$ and the variation δH yields to quadratic equations.

$$\delta H(u, v, w, \mathbf{N}) = \int_\Omega (\mathbf{N}\colon \delta\boldsymbol{\Gamma} + (\boldsymbol{\Gamma} - \mathbf{N}\colon \mathbf{C}_m^{-1})\colon \delta\mathbf{N} + \boldsymbol{\kappa}\colon \mathbf{C}_b \colon \delta\boldsymbol{\kappa})\, \mathrm{d}\Omega. \tag{6a}$$

The variational principle $\delta H(u, v, w, \mathbf{N}) = 0$ is equivalent to

$$\begin{cases} \delta P(u, v, w) = 0 & \text{the virtual work principle,} \\ \mathbf{N} = [\mathbf{C}_m]\colon \boldsymbol{\Gamma} & \text{the constitutive equation.} \end{cases} \tag{6b}$$

When working with the power series expansion, it was found better to use the functional H which leads to a quadratic non-linearity. As for the kinetic energy T of the plate, the rotatory inertia terms are neglected, which is the most usual procedure for plate deflection. This gives the following functional:

$$T = \frac{1}{2}\int_\Omega \rho h(\dot{u}^2 + \dot{v}^2 + \dot{w}^2)\, \mathrm{d}\Omega, \tag{7}$$

in which ρ is the mass density and the overdot means the differentiation with respect to time.

2.2. HARMONIC BALANCE METHOD AND OPERATIONAL FORMULATION

In the present work, only periodic vibrations of an undamped system are considered. For a simple representation, harmonic motion is studied in a simple way. Assume that the displacement vector is given by:

$$\begin{cases} u(x, y, t) = u(x, y) \sin^2 \omega t, \\ v(x, y, t) = v(x, y) \sin^2 \omega t, \\ w(x, y, t) = w(x, y) \sin \omega t, \end{cases} \tag{8}$$

where ω is the natural frequency. Insertion of (8) into (2) leads to the formulation of strains, curvature and membrane tensors as follow:

$$\begin{cases} \boldsymbol{\Gamma}^L(x, y, t) = \boldsymbol{\gamma}^L(x, y) \sin^2 \omega t, \\ \boldsymbol{\Gamma}^{NL}(x, y, t) = \boldsymbol{\gamma}^{NL}(x, y) \sin^2 \omega t, \\ \boldsymbol{\kappa}(x, y, t) = \boldsymbol{\kappa}(x, y) \sin \omega t, \\ \mathbf{N}(x, y, t) = \mathbf{N}(x, y) \sin^2 \omega t, \end{cases} \tag{9a}$$

in which

$$\mathbf{N} = [\mathbf{C}_m] : \boldsymbol{\gamma} \quad \text{and} \quad \boldsymbol{\gamma} = \boldsymbol{\gamma}^L + \boldsymbol{\gamma}^{NL}. \tag{9b}$$

Equation (5a) giving the strain energy becomes:

$$H(u, v, w, \mathbf{N}) = \sin^4 \omega t \int_\Omega [\mathbf{N} : \boldsymbol{\gamma} - \frac{1}{2} \mathbf{N} : \mathbf{C}_m^{-1} : \mathbf{N}] \, d\Omega$$

$$+ \sin^2 \omega t \int_\Omega \frac{1}{2} \boldsymbol{\kappa} : \mathbf{C}_b : \boldsymbol{\kappa} \, d\Omega. \tag{10}$$

To study the history of the actual solution corresponding to a period, we set the initial time $t_1 = 0$ and the final time $t_2 = 2\pi/\omega$. After integration over the time range one obtains:

$$\int_0^{2\pi/\omega} (H - T) \, dt = \frac{\pi}{\omega} \left\{ \frac{3}{4} \int_\Omega \left(\mathbf{N} : \boldsymbol{\gamma} - \frac{1}{2} \mathbf{N} : \mathbf{C}_m^{-1} : \mathbf{N} \right) d\Omega \right.$$

$$\left. + \frac{1}{2} \int_\Omega \boldsymbol{\kappa} : \mathbf{C}_b : \boldsymbol{\kappa} \, d\Omega - \omega^2 \frac{1}{2} \rho h \int_\Omega (u^2 + v^2 + w^2) \, d\Omega \right\}. \tag{11}$$

Using Hamilton's principle, the governing equation is given by:

$$\frac{3}{4}\int_{\Omega}(\delta\boldsymbol{\gamma}\colon \mathbf{N} + \delta\mathbf{N}\colon \boldsymbol{\gamma} - \delta\mathbf{N}\colon \mathbf{C}_m^{-1}\colon \mathbf{N})\,\mathrm{d}\Omega$$

$$+\int_{\Omega}\delta\boldsymbol{\kappa}\colon \mathbf{C}_b\colon \boldsymbol{\kappa}\,\mathrm{d}\Omega - \omega^2\rho h\int_{\Omega}(u\delta u + v\delta v + w\delta w)\,\mathrm{d}\Omega = 0. \quad (12)$$

This mixed variational principle can be used directly by using a mixed finite element method. To obtain a displacement formulation one can determine the membrane stress $\mathbf{N}$ as a function of the displacement.

$$\mathbf{N}(x, y) = [\mathbf{C}_m][\boldsymbol{\gamma}(u, v, w)] = [\mathbf{C}_m][\boldsymbol{\gamma}^L(u, v) + \boldsymbol{\gamma}^{NL}(w, w)]. \quad (13)$$

The insertion of the stress $\mathbf{N}$ into equation (12) leads to a variational principle of cubic non-linearity in displacement. After discretization by the finite element method, one gets a non-linear eigenvalue problem. This problem could be treated by a predictor-corrector method. Our purpose here is to solve the variational equation (12) using an asymptotic-numerical method.

Introduce the following change of variables which represents a perturbation of the frequency parameter ω in the vicinity of a linear eigenfrequency ω_L by:

$$\omega^2 = \omega_L^2 + \varepsilon. \quad (14)$$

Inserting equation (14) into the equilibrium equation (12) gives:

$$\frac{3}{4}\int_{\Omega}[\mathbf{N}\colon \delta\boldsymbol{\gamma}^L + (\boldsymbol{\gamma}^L - \mathbf{C}_m^{-1}\colon \mathbf{N})\colon \delta\mathbf{N}]\,\mathrm{d}\Omega + \int_{\Omega}\delta\boldsymbol{\kappa}\colon \mathbf{C}_b\colon \boldsymbol{\kappa}\,\mathrm{d}\Omega$$

$$-\omega_L^2\rho h\int_{\Omega}[u\delta u + v\delta v + w\delta w]\,\mathrm{d}\Omega - \varepsilon\rho h\int_{\Omega}[u\delta u + v\delta v + w\delta w]\,\mathrm{d}\Omega$$

$$+\frac{3}{4}\int_{\Omega}[\mathbf{N}\colon \delta\boldsymbol{\gamma}^{NL} + \boldsymbol{\gamma}^{NL}\colon \delta\mathbf{N}]\,\mathrm{d}\Omega = 0. \quad (15)$$

In view of using an operational notation as presented in references [36–39, 42], the governing equation (15) can be written as:

$$\langle \mathbf{L}\cdot\mathbf{U}, \delta\mathbf{U}\rangle - (\omega^2 - \omega_L^2)\langle \mathbf{M}\cdot\mathbf{U}, \delta\mathbf{U}\rangle + \langle \mathbf{Q}(\mathbf{U}, \mathbf{U}), \delta\mathbf{U}\rangle = 0, \quad (16a)$$

in which $\mathbf{U} = {}^t[u, v, w, \mathbf{N}]$ is the mixed vector and

$$\langle \mathbf{L}\cdot\mathbf{U}, \delta\mathbf{U}\rangle = \frac{3}{4}\int_{\Omega}[\mathbf{N}\colon \delta\boldsymbol{\gamma}^L + (\boldsymbol{\gamma}^L - \mathbf{C}_m^{-1}\colon \mathbf{N})\colon \delta\mathbf{N}]\,\mathrm{d}\Omega + \int_{\Omega}\delta\boldsymbol{\kappa}\colon \mathbf{C}_b\colon \boldsymbol{\kappa}\,\mathrm{d}\Omega$$

$$-\omega_L^2\rho h\int_{\Omega}[u\delta u + v\delta v + w\delta w]\,\mathrm{d}\Omega, \quad (16b)$$

$$\langle \mathbf{M} \cdot \mathbf{U}, \delta\mathbf{U} \rangle = \rho h \int_{\Omega} [u\delta u + v\delta v + w\delta w] \, \mathrm{d}\Omega, \tag{16c}$$

$$\langle \mathbf{Q}(\mathbf{U}, \mathbf{U}), \delta\mathbf{U} \rangle = \frac{3}{4} \int_{\Omega} [\mathbf{N}: \delta\boldsymbol{\gamma}^{NL} + \boldsymbol{\gamma}^{NL}: \delta\mathbf{N}] \, \mathrm{d}\Omega. \tag{16d}$$

The operators $\mathbf{L}$ and $\mathbf{M}$ are linear and $\mathbf{Q}$ is a quadratic one. The matrices corresponding to the operators $\mathbf{L}$ and $\mathbf{M}$ are the linear stiffness and the mass matrices, respectively.

3. ASYMPTOTIC-NUMERICAL METHOD

The asymptotic numerical method has been successfully used to study the buckling and post-buckling of elastostatic structures like beams, plates and shells [35–41]. The backbone curve that determines the free vibration analysis of plates is a branch that bifurcates from the fundamental solution $\mathbf{U} = 0$ at $\omega = \omega_{\mathrm{L}}$, where ω_L is the linear frequency of vibration. At the bifurcation point ($\mathbf{U} = 0$, $\omega = \omega_L$), the tangent operator $\mathbf{L}$ is singular. Furthermore, it is assumed that the kernel of this tangent operator is one-dimensional, which generally occurs. Using the Lyapunov–Schmidt reduction method and implicit function theorem it can be established that the unknown vector $\mathbf{U}$ and the frequency parameter ω can be expanded into integro-power series of a parameter a in the vicinity of the bifurcating point as follows [38, 42].

$$\begin{cases} \mathbf{U} = a\mathbf{U}_1 + \sum_{p=2}^{+\infty} a^p \mathbf{U}_p, & \text{(17a)} \\ \omega^2 = \omega_L^2 + \sum_{p=1}^{+\infty} a^p C_{(p)}, & \text{(17b)} \\ \langle \mathbf{U}^1, \mathbf{U}_p \rangle = 0 \quad \text{if} \quad p > 1. & \text{(17c)} \end{cases}$$

Hence, $\mathbf{U}_p$ are mixed unknown vectors and $C_{(p)}$ are unknown coefficients. The orthogonality condition (17c) is obtained from Lyapunov–Schmidt reduction and from the assumption that the kernel of the tangent operator $\mathbf{L}$ is one-dimensional and generated by the vector $\mathbf{U}_1$. Introducing equation (17) into equation (16a) and equating like powers of a, one obtains the following set of linear mixed problems.

$$\begin{aligned} &\text{order 1} \quad \mathbf{L} \cdot \mathbf{U}_1 = 0, \\ &\text{order 2} \quad \mathbf{L} \cdot \mathbf{U}_2 = \mathbf{C}_{(1)}\mathbf{M} \cdot \mathbf{U}_1 - \mathbf{Q}(\mathbf{U}_1, \mathbf{U}_1), \\ &\ldots\ldots \\ &\text{order p} \quad \mathbf{L} \cdot \mathbf{U}_p = \sum_{r=1}^{p-1} \mathbf{C}_{(r)}\mathbf{M} \cdot \mathbf{U}_{p-r} - \sum_{r=1}^{p-1} \mathbf{Q}(\mathbf{U}_r, \mathbf{U}_{p-r}). \end{aligned} \tag{18}$$

The principle of this numerical method is to compute successively a number of vectors $\mathbf{U}_p$ and coefficients $C_{(p)}$ up to a given order n. The truncature of the series (17) at the order n yields polynomials $\omega(a, n)$ and $\mathbf{U}(a, n)$ that are considered as approximations of the exact solution branch.

Order 1. Solve the following variational problem

$$\langle \mathbf{L} \cdot \mathbf{U}_1, \delta\mathbf{U} \rangle = 0. \tag{19}$$

The resolution of this problem gives the linear vibration modes. This allows one to determine the linear frequency ω_L and the corresponding vibration mode $\mathbf{U}_1$.

Order p. To compute the vector $\mathbf{U}_p$, the only difficulty is to construct the right-hand sides which depends on $\mathbf{U}_q$ and $C_{(q)}$, $q < p$. The detail of the construction of the right-hand side is given in Appendix A. The pth problem can be written under the more compact form:

$$\langle \mathbf{L} \cdot \mathbf{U}_p; \delta\mathbf{U} = \langle \mathbf{F}_{(p)}, \delta\mathbf{U} \rangle \quad \forall \delta U, \tag{20a}$$

$$\langle \mathbf{U}_p; \mathbf{U}_1 \rangle = 0 \qquad \text{for} \quad p > 1, \tag{20b}$$

$$C_{(p-1)} = \frac{1}{\langle \mathbf{M} \cdot \mathbf{U}_1, \mathbf{U}_1 \rangle} \left\{ - \sum_{r=1}^{p-2} C_{(p)} \langle \mathbf{M} \cdot \mathbf{U}_{p-r}; \mathbf{U}_1 \rangle \right.$$

$$\left. + \sum_{r=1}^{p-1} \langle \mathbf{Q}(\mathbf{U}_r, \mathbf{U}_{p-r}); \mathbf{U}_1 \rangle \right\}. \tag{20c}$$

Note that the coefficient $C_{(p)}$ is computed in terms of the vectors $\mathbf{U}_q$, $q \leqslant p$ and $C_{(p)}$ takes place in the determination of $\mathbf{U}_{p+1}$.

Recall that the unknown vector $\mathbf{U}_p$ includes not only the displacements u, v and w but also the membrane stress resultant $N_{\alpha\beta}$ which had been introduced to reduce the order of the non-linearity to a quadratic one in the governing equation. As a consequence, all the linear problems (20) are mixed. In order to use classical FEM, equations (20) are transformed into a pure displacement problem and a pseudo-constitutive equation which gives the pth term of the resultant stress $\mathbf{N}_{(p)}$. To get $\mathbf{N}_{(p)}$ at order p, put $\delta u = \delta v = \delta w = 0$ and $\delta N_{\alpha\beta} \neq 0$ in equations (20) to yield:

$$\mathbf{N}_{(p)} = [\mathbf{C}_m][\boldsymbol{\gamma}^L_{(p)} - \mathbf{F}^N_{(p)}], \tag{21}$$

where $\mathbf{F}^N_{(p)}$ is given in Appendix A.

The resultant stress $\mathbf{N}_{(p)}$ is obtained as a function of the displacement. The insertion of equation (21) into equations (20) leads to a pure displacement problem as follows.

Denote the displacement vector $\bar{\mathbf{U}}$ by:

$$\bar{\mathbf{U}} = \begin{Bmatrix} u \\ v \\ w \end{Bmatrix}, \tag{22}$$

$$\langle \bar{\mathbf{L}} \cdot \bar{\mathbf{U}}_P; \delta\bar{\mathbf{U}} \rangle = \langle \bar{\mathbf{F}}_p; \delta\bar{\mathbf{U}} \rangle \quad \forall \delta\bar{\mathbf{U}}, \tag{23a}$$

$$\langle \bar{\mathbf{U}}_p; \bar{\mathbf{U}}_1 \rangle = 0 \qquad \text{for} \quad p > 1, \tag{23b}$$

with

$$\langle \bar{\mathbf{L}} \cdot \bar{\mathbf{U}}_p, \delta\bar{\mathbf{U}} \rangle = \frac{3}{4} \int_\Omega \boldsymbol{\gamma}^L \colon \mathbf{C}_m \colon \delta\boldsymbol{\gamma}^L \, \mathrm{d}\Omega + \int_\Omega \boldsymbol{\kappa} \colon \mathbf{C}_b \colon \delta\boldsymbol{\kappa} \, \mathrm{d}\Omega$$

$$- \omega_L^2 \rho h \int_\Omega (u\delta u + v\delta v + w\delta w) \, \mathrm{d}\Omega, \tag{24a}$$

$$\langle \bar{\mathbf{F}}_{(p)}, \delta\bar{\mathbf{U}} \rangle = \int_\Omega (\mathbf{F}^U_{(p)} \delta\bar{\mathbf{U}} + \frac{3}{4} F^W_{\alpha(p)} \delta w, \alpha + \frac{3}{4} \mathbf{C}_m \colon \mathbf{F}^N_{(p)} \colon \delta\boldsymbol{\gamma}^L) \, \mathrm{d}\Omega, \tag{24b}$$

where , $\mathbf{F}^U$, F^w_α and $\mathbf{F}^N$ are given in Appendix A.

The operator $\langle \bar{\mathbf{L}} \cdot \bar{\mathbf{U}}p, \delta\bar{\mathbf{U}} \rangle$ is similar to an operator of dynamical stiffness and it involves the elastic bending stiffness, the membrane stiffness and the mass operator. So, the mixed problem (20) has been replaced by the displacement problem (23) and the constitutive equation (21) giving the stress. Finally, $\mathbf{N}$ is a convenient additional variable for reducing the equation degree and to make the expansion procedure easier. Once the non-linear problem is transformed into a set of linear problems, the stress is eliminated and a classical FEM is used to solve the linear problems.

3.1. LINEAR VIBRATION (U_1, ω_L)

Before computing the vectors $\bar{\mathbf{U}}_p$ and the coefficients $C_{(p)}$ that give the backbone curve, one must determine the eigenmode and eigenfrequency characterising the linear vibrations. To do so, it is necessary to solve equation (19), written in a displacement form as follows:

$$\langle \bar{\mathbf{L}} \cdot \bar{\mathbf{U}}_1, \delta\bar{\mathbf{U}} \rangle = 0. \tag{25a}$$

With the classical notation of computational mechanics [43, 44] the discretization of this problem leads to an eigenvalue problem in the form:

$$[\mathbf{K}e - \omega_L^2 \mathbf{M}][\bar{\mathbf{U}}_1] = 0, \tag{25b}$$

where $[\mathbf{K}e]$ is the elastic stiffness matrix and $[\mathbf{M}]$ is the mass matrix. The solution of this problem gives the linear modes and linear frequencies of vibration. Denote by $[\bar{\mathbf{U}}_1]$ the first mode of vibration and ω_L its corresponding frequency.

3.2. COMPUTATION OF $\bar{\mathbf{U}}_p$ AND $C_{(p)}$

The discretization of the problem (23a) reads

$$[\mathbf{K}e - \omega_L^2 \mathbf{M}][\bar{\mathbf{U}}_p] = [\bar{\mathbf{F}}_{(p)}], \tag{26}$$

in which $[\bar{\mathbf{U}}_p]$ is the vector of the modal displacement of order p. $[\mathbf{K}e - \omega_L^2 \mathbf{M}]$ is the tangent stiffness matrix at a bifurcation point which is singular. The

orthogonality condition (23b) between $\bar{\mathbf{U}}_p$ and $\bar{\mathbf{U}}_1$ should be added to equation (26) in order to get an invertible problem. After discretization, this condition reads:

$$[\bar{\mathbf{U}}_1]^t \cdot [\mathbf{P}] \cdot [\bar{\mathbf{U}}_p] = 0. \tag{27}$$

where $\mathbf{P}$ is a positive-definite matrix associated with the scalar product (23b). Now choose $[\mathbf{P}] = [\mathbf{K}e]$ to have an energy oriented scalar product. So, after relaxation of equation (26) by equation (27) an invertible problem is obtained [35–39, 42].

$$\left[\begin{array}{c|c} \mathbf{K}e - \omega_L^2 \mathbf{M} & \bar{\mathbf{U}}^* \\ \hline \bar{\mathbf{U}}^{*t} & \mathbf{0} \end{array}\right] \left[\begin{array}{c} \bar{\mathbf{U}}_p \\ \hline k \end{array}\right] = \left[\begin{array}{c} \bar{\mathbf{F}}_{(p)} \\ \hline \mathbf{0} \end{array}\right], \tag{28}$$

where $[\bar{\mathbf{U}}^*] = [\mathbf{K}e][\bar{\mathbf{U}}_1]$ and k is a Lagrange multiplier. Notice that the stiffness matrix is the same for all linear problems. Hence, a Crout decomposition is performed once for all. The right hand side vector $\bar{\mathbf{F}}_{(p)}$ depends on the already calculated vectors $\mathbf{U}_q$ and coefficients $C_{(q)}$ for $q < p$. The assembling of $\bar{\mathbf{F}}_{(p)}$ is very similar to the assembling of a residual vector in a Newton–Raphson scheme and requires about the same computation time. The computation of the coefficients $C_{(p)}$ and the membrane stress $N_{\alpha\beta(p)}$ can be judiciously performed during the assembling of the right-hand side. $\bar{\mathbf{F}}$, so, that almost no additional computation time is required for these quantities.

In summary, this asymptotic-numerical method requires about the same computation time as a modified Newton–Raphson step with $(n-1)$ iterations without recalculating the stiffness matrix. The computation time of some vectors $\mathbf{U}_p$ in the static case with elastic analysis, buckling analysis and Newton–Raphson steps have been given in Table 1 of reference [39]. For a large number of d.o.f., most of the computing time is spent in the Crout decomposition. This is why the computation of many terms requires only 50% of additional computation time compared to a linear analysis.

Finally, the linear and non-linear vibrations of plates with various shapes and boundary conditions can be easily studied. The numerical solution of the eigenvalue problem (25b) gives the linear frequency ω_L and linear mode U_1. Obviously, the other frequencies and associated mode shapes are computed. To obtain the non-linear frequency and the non-linear mode shape, one has to solve the set of linear systems (28). This leads to the computation of the displacement vectors $\bar{\mathbf{U}}_p = \{u_p, v_p, w_p\}$, the associated stress $\mathbf{N}_{(p)} = \{N_{xx(p)}, N_{yy(p)}, N_{xy(p)}\}$ and the coefficients $C_{(p)}$ constituting the frequency for each order p. The truncation of the series (17) at order n gives:

$$\begin{cases} \omega^2(a) = \omega_L^2 + aC_{(1)} + a^2 C_{(2)} + \cdots + a^n C_{(n)}, \\ \bar{\mathbf{U}}(a) = a\mathbf{U}_1 + a^2\mathbf{U}_2 + a^3\mathbf{U}_3 + \cdots + a^n\mathbf{U}_n, \\ \mathbf{N}(a) = a\mathbf{N}_{(1)} + a^2\mathbf{N}_{(2)} + a^3\mathbf{N}_{(3)} + \cdots + a^n\mathbf{N}_{(n)}. \end{cases} \tag{29}$$

TABLE 1

Frequency ratio ω/ω_L according to the maximum amplitude $w^* = w(centre)/h$ for a simply supported isotropic square plate ($v = 0.3$)

	ω/ω_L							
w^*	Present study ANM	FEM + incremental method [21]	1-mode + Gauss integration [8]	1-mode + Runge–Kutta [6]	1-mode + elliptic integrals [1, 3]	1-mode + perturbation method [1, 3, 19]	Rayleigh–Ritz method [12]	FEM + linearisation [17]
0·2	1·01976	1·0196	1·0189	1·0208	1·0195	1·0196	1·0149	1·0134
0·4	1·07669	1·0763	1·0771	1·0805	1·0757	1·0761	1·0583	1·0528
0·6	1·16596	1·1645	1·1669	1·1725	1·1625	1·1642	1·1270	1·1154
0·8	1·28124	1·2779	1·2813	1·2894	1·2734	1·2774	1·2166	1·1979
1·0	1·41666	1·4109	1·4141	1·4248	1·4024	1·4097	1·3230	1·2967

TABLE 2

Frequency ratio ω/ω_L according to the maximum amplitude $w^* = w(centre)/h$ for a fully clamped isotropic square plate ($v = 0.3$)

	ω/ω_L							
w^*	Present study ANM	Multi-mode analysis [25, 26)	Perturbation method [1]	FEM + incremental method [21]	M. Sathy-amoorthy[a]	G. V. Rao *et al.*[a]	J. N. Reddy[a]	C. Mei[a]
0·2	1·00723	1·0070	1·0085	1·0073	1·0129	1·0070	1·0062	1·0062
0·4	1·02860	1·0276	1·0292	1·0291	1·0306	1·0276	1·0245	1·0256
0·6	1·06321	1·0607	1·0661	1·0648	1·0665	1·0608	1·0540	1·0564
0·8	1·10975	1·1044	1·1136	1·1138	1·1157	1·1047	1·0934	1·0970
1·0	1·16672	1·1573	1·1674	1·1762	1·1684	1·1578	1·1411	1·1429

[a] Values taken from references [25, 26].

These series permit one to obtain the frequency (or the period) as a function of the displacement at any desired point of the plate. The membrane stress or bending stress can also be easily obtained.

3.3. NUMERICAL RESULTS

To bring out the effectiveness and reliability of this method, numerical results of non-linear free vibrations of thin elastic plates with various shapes and boundary conditions will be presented. The linear problems (25b) and (28) are solved using the classical finite element method. The plate is modelled with triangular shell elements D.K.T. which have three nodes and five d.o.f. per node $(u, v, w, \theta_1, \theta_2)$ [43, 44]. These investigations give the linear frequency ω_L, the associated mode shape (u_1, v_1, w_1) and the vectors $\bar{\mathbf{U}}_p = {}^t\{u_p, v_p, w_p\}$ at each order p. The coefficients $C_{(p)}$ are obtained by the algebraic equation (20c) and the stress vectors $\mathbf{N}_{(p)}$ are given by equation (21). The non-linear frequency ω, the non-linear displacement (u, v, w) and the associated stress are obtained by the series (29). Only the order n of the truncation has to be chosen. The truncation of these series at order 2 gives the same results as those obtained by the assumed one-mode analysis and perturbation method for the resulting Duffing equation. A comparison with the previously published results for a simply supported and a fully clamped square plate is given in Tables 1 and 2. A good agreement can be seen between the present results and those of various authors. The assumed one-mode analysis gives a good prediction of the non-linear frequency corresponding to the maximum amplitude, especially for the simply supported case. This analysis, which is generally used, remains efficient particularly when the interaction between higher modes is very small. The major disadvantage of the one-mode analysis is that the predicted deformation is proportional to the linear mode. This leads to inaccurate results, as will be shown later. In Figures 1 and 2, are presented the deflection at the centre $w(centre)/h$ versus the frequency ratio ω/ω_L for different orders of truncation (12–14–16–18) of the series (29) for a fully clamped square plate and at orders (18–20) for a fully clamped circular plate. Published results, obtained by the multi-mode analysis [25, 26] and by the FEM and iteration process [15, 21] are added for comparison. It is apparent that the extension of the backbone curves is in good agreement with these results.

The frequency–displacement curves given by the series (29) are very characteristic of polynomial approximations. Indeed, for small values of the parameter a, the asymptotic-numerical solutions (29) coincide quite perfectly until a critical value of a. Beyond this value the truncated polynomial series separate from each other and diverge. Obviously, this critical value is *the radius of convergence* of the series (29) (see Figures 1 and 2). The limitation of the validity of the solution is not a handicap of this method for two main reasons. First, the zone of convergence is sufficiently large. As presented in Figure 1, one obtains a large part of the backbone curve characterising the non-linear vibrations of a fully clamped square plate until $\omega \cong 1{\cdot}3\omega_L$ and $w(centre) \cong 1{\cdot}5h$. Second, the range of validity of the asymptotic solutions can be easily increased by using some shrewd strategies like the continuation techniques [41] or the Padé approximants [38–40]. The effectiveness of these procedures will be presented in the following sections.

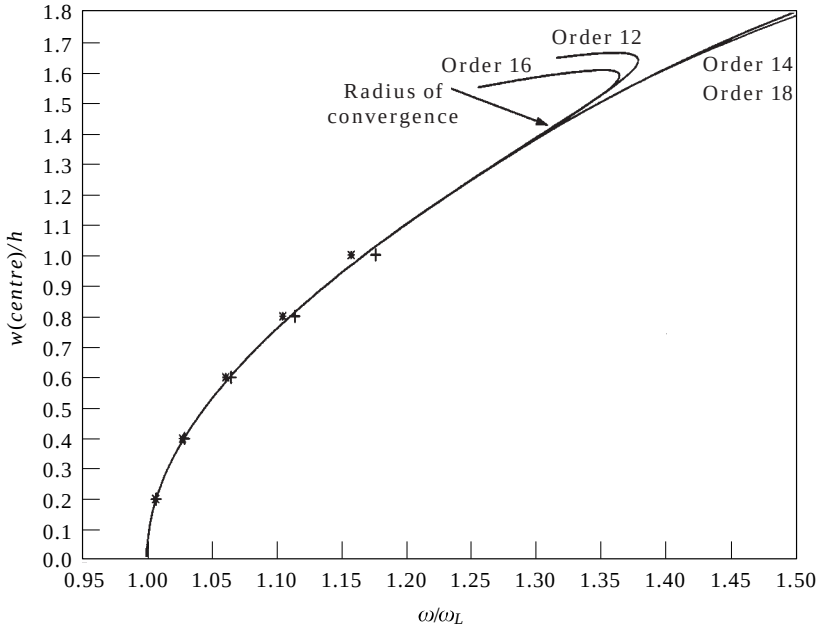

Figure 1. Displacement–frequency curve for a fully clamped square plate: (——) $w(centre)/h$ versus the frequency ratio ω/ω_L at different orders of the truncation of the asymptotic numerical solution (29). (orders: 12–14–16–18); (*) indicates the results of references [25, 26] and (+) indicates the results of reference [21].

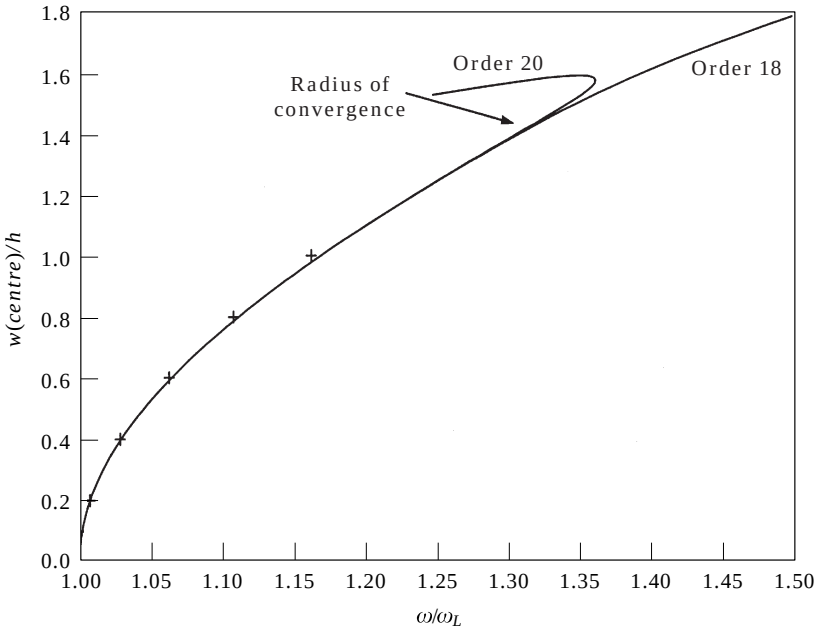

Figure 2. Displacement–frequency curve for a fully clamped circular plate: (——) $w(centre)/h$ versus the frequency ration ω/ω_L at orders 18–20 of the truncation of the series (29). (+) indicates the results of reference [15].

4. IMPROVEMENT OF THE SOLUTION

The asymptotic numerical method gives an analytical solution as a function of the perturbed parameter. It has been shown in Figures 1 and 2 that the validity of the solution is limited by a radius of convergence. This is clearly defined in all the studied cases and depends on the rigidity of the structure. Nevertheless, the part of the backbone curve obtained is sufficiently large for the initial non-linear vibrations [42]. For large vibration amplitudes, one has to overcome this limitation. This is the main objective of the following sections. Two useful strategies are presented that have been successfully tested in the static post-buckling analysis.

4.1. CONTINUATION PROCEDURE

The polynomial solutions (29) coincide perfectly inside the radius of convergence but they diverge out of this zone of validity. This limit can be computed automatically following the same procedure as presented by Cochelin [41]. A simple criterion is that the difference between two constitutive order solutions remains small.

$$\frac{\|\mathbf{U}_{\text{order}n} - \mathbf{U}_{\text{order}(n-1)}\|}{\|\mathbf{U}_{\text{order}n}\|} = \frac{\|a^n\mathbf{U}_n\|}{\|a\mathbf{U}_1 + a^2\mathbf{U}_2 + \cdots + a^n\mathbf{U}_n\|} \leqslant \varepsilon. \tag{30}$$

Here, ε is a small number. By approximating the denominator as $\|a\mathbf{U}_1\|$, one obtains a simple criterion in displacement.

$$a_{limit} = \varepsilon\left(\frac{\|\mathbf{U}_1\|}{\|\mathbf{U}_n\|}\right)^{1/n-1}. \tag{31}$$

Note that this simple criterion gives a good order of magnitude of the validity of the solution, whereas it requires almost no computing time. However, a more secure way of controlling the quality of the asymptotic solution consists of computing residual vectors. Anyway, the simple criterion given above is very helpful in defining the range of interest of the parameter a and it was successfully tested in various studies [41].

Taking a starting point in the zone of validity of the solution, one can reapply the ANM and go far into the solution path. Although, the continued solution has a radius of convergence, the application of the ANM iteratively allows one to determine a complex non-linear branch by a succession of local asymptotic expansions.

4.1.1. *The path-following algorithm*

The ANM presented above started at the bifurcating point ($\mathbf{U} = 0$, $\omega = \omega_L$). This permitted the backbone curve to be obtained up to the radius of convergence. In this section, the starting point will be taken in the zone of validity of the solution and the ANM reapplied. Denote the starting point by ($\mathbf{U}_0$, ω_0) and develop the solution in the neighbourhood of this point.

$$\mathbf{L}\cdot\mathbf{U} - (\omega^2 - \omega_0^2)\mathbf{M}\cdot\mathbf{U} + \mathbf{Q}(\mathbf{U}, \mathbf{U}) = 0, \tag{32a}$$

$$\begin{cases} \mathbf{U} = \mathbf{U}_0 + a\mathbf{V}_1 + a^2\mathbf{V}_2 + a^3\mathbf{V}_3 + \cdots + a^p\mathbf{V}_p + \cdots, \\ \omega^2 = \omega_0^2 + a\omega_{(1)} + a^2\omega_{(2)} + a^3\omega_{(3)} + \cdots + a^p\omega_{(p)} + \cdots, \end{cases} \tag{32b}$$

in which $\mathbf{V}_p$ and $\omega_{(p)}$ are the new unknowns of the problem (32a). Introducing (32b) into (32a) and equating like powers of a, one obtains the following set of linear problems:

$$\begin{aligned} &\text{order 1:} \quad \mathbf{L}_t \cdot \mathbf{V}_1 = \omega_{(1)}\mathbf{M} \cdot \mathbf{U}_0, \\ &\text{order 2:} \quad \mathbf{L}_t \cdot \mathbf{V}_2 = \omega_{(2)}\mathbf{M} \cdot \mathbf{U}_0 + \omega_{(1)}\mathbf{M} \cdot \mathbf{V}_1 - \mathbf{Q}(\mathbf{V}_1, \mathbf{V}_1), \\ &\cdots \\ &\text{order } p\text{:} \quad \mathbf{L}_t \cdot \mathbf{V}_p = \omega_{(p)}\mathbf{M} \cdot \mathbf{U}_0 + \sum_{r=0}^{p-2} \omega_{(r+1)}\mathbf{M} \cdot \mathbf{V}_{p-r-1} - \sum_{r=1}^{p-1} \mathbf{Q}(\mathbf{V}_r, \mathbf{V}_{p-r}), \end{aligned} \tag{33}$$

in which the tangent operator $\mathbf{L}_t$ is defined as $\mathbf{L}_t(\,\cdot\,) = \mathbf{L}(\,\cdot\,) + 2\mathbf{Q}(\mathbf{U}_0, \cdot\,)$. The first equation corresponds to the linearisation of equation (32a) at the starting point $(\mathbf{U}_0, \omega_0)$, i.e., the vector $\mathbf{V}_1$ and the coefficient $\omega_{(1)}$ correspond to the tangent of the branch at the starting point. Notice that at each order p both $\mathbf{V}_p$ and $\omega_{(p)}$ are unknown and there is one superfluous unknown in each of these linear problems. So, one must add a solvability equation. Therefore, it is better to consider a measure that includes the entire displacement vector and also the load parameter, i.e., an arc length measure [45–47].

Following this idea, the path parameter a will be identified as the projection of the displacement increment $(\mathbf{U}(a) - \mathbf{U}_0)$ and the load increment $(\omega(a) - \omega_0)$ on the tangent vector $(\mathbf{V}_1, \omega_{(1)})$ [41].

$$a = \frac{1}{s^2}\{\langle \mathbf{U} - \mathbf{U}_0, \mathbf{V}_1 \rangle + (\omega - \omega_0)\omega_{(1)}\}. \tag{34}$$

Here $\langle\,\cdot\,,\,\cdot\,\rangle$ is the Euclidean scalar product and s is a scaling parameter which corresponds to the length of the tangent vector $(\mathbf{V}_1, \omega_{(1)})$. Introducing the series (32b) into equation (34) and equating like powers of a, one obtains the following set of single equations

$$\begin{aligned} &\text{order 1:} \quad \langle \mathbf{V}_1, \mathbf{V}_1 \rangle + \omega_{(1)}\omega_{(1)} = s^2, \\ &\text{order 2:} \quad \langle \mathbf{V}_1, \mathbf{V}_2 \rangle + \omega_{(1)}\omega_{(2)} = 0, \\ &\text{order 3:} \quad \langle \mathbf{V}_1, \mathbf{V}_3 \rangle + \omega_{(1)}\omega_{(3)} = 0, \\ &\text{order } p\text{:} \quad \langle \mathbf{V}_1, \mathbf{V}_p \rangle + \omega_{(1)}\omega_{(p)} = 0. \end{aligned} \tag{35}$$

Finally, all vectors $\mathbf{V}_p$ and coefficients $\omega_{(p)}$ of the series (32b) can be determined by successively solving the systems of equations (33) and (35) at each order p.

Now, recall that the new unknown vectors $\mathbf{V}_p$ are mixed. Following the same manipulation presented in section 3, return to a pure displacement formulation. After discretization, one obtains the following matrix problem:

$$\begin{cases} [\mathbf{K}_t(\mathbf{U}_0)]\{\mathbf{V}_p\} = \omega_{(p)}\{\mathbf{F}\} + \{\mathbf{F}_p^{NL}\}, \\ \langle \mathbf{V}_1, \mathbf{V}_p \rangle + \omega_{(1)}\omega_{(p)} = 0, \end{cases} \tag{36}$$

where $[\mathbf{K}_t(\mathbf{U}_0)]$ is the tangent stiffness matrix at the starting point $(\mathbf{U}_0, \omega_0)$, $\{\mathbf{F}\}$ is the column vector $(\mathbf{M} \cdot \mathbf{U}_0)$, and $\{\mathbf{F}_p^{NL}\}$ represents the remaining part of the right-hand side of equations (33). The problem (36) is solved in the following steps:

step 1: solve $[\mathbf{K}_t(\mathbf{U}_0)]\{\mathbf{V}_1^L\} = \{\mathbf{F}\}$,

step 2: compute $\omega_{(1)} = \pm \dfrac{s}{\sqrt{\langle \mathbf{V}_1^L, \mathbf{V}_1^L \rangle + 1}}, \qquad \mathbf{V}_1 = \omega_{(1)}\mathbf{V}_1^L,$ (37b)

step 3: compute $\mathbf{N}_{(1)} = [\mathbf{C}_m][\boldsymbol{\gamma}^L(\mathbf{V}_1) + 2\boldsymbol{\gamma}^{NL}(\mathbf{U}_0, \mathbf{V}_1)]$ (37c)

Order p

step 1: solve $[\mathbf{K}_t(\mathbf{U}_0)]\{\mathbf{V}_p^{NL}\} = \{\mathbf{F}_p^{NL}\},$ (38a)

step 2: compute $\omega_{(p)} = -\dfrac{\langle \mathbf{V}_1, \mathbf{V}_p^{NL} \rangle}{s^2}\,\omega_{(1)}, \quad \mathbf{V}_p = \dfrac{\omega_{(p)}}{\omega_{(1)}}\,\mathbf{V}_1 + \mathbf{V}_p^{NL},$ (38b)

step 3: compute $\mathbf{N}_{(p)} = [\mathbf{C}_m][\boldsymbol{\gamma}^L(\mathbf{V}_p) + 2\boldsymbol{\gamma}^{NL}(\mathbf{U}_0, \mathbf{V}_p) + \sum_{r=1}^{p-1} \boldsymbol{\gamma}^{NL}(\mathbf{V}_r, \mathbf{V}_{p-r})].$ (38c)

Once again, the linear problems obtained have the same tangent matrix that one has to invert once for all different orders. So, all unknown terms of the series (32b) can be easily obtained. Using this method, the range of validity of the first series (29) is extended. Obviously, the new series also has a radius of convergence, but the reapplication of this process as many times as required removes the problem of limitation.

Finally, it is shown that this method can be applied iteratively in a step by step manner. Because of the local analytical representation of the branch within each step, the present path following technique has some important advantages compared to classical predictor-corrector schemes.

4.2. Padé approximations

In this section it is shown that the computed series (29) can be *a posteriori* transformed into a much more accurate approximation of the exact solution. It is also shown in numerical results of free vibrations of plates that the series (29) fails beyond the radius of convergence (see Figures 1 and 2). An obvious reason to explain this failure could be that the n first vectors $\mathbf{U}_{(p)}$ form a too poor basis to represent the branch. To go further, one has to go through an orthogonalization process in order to obtain a more complete orthogonal basis. The obtained orthogonal basis seems to be more accurate. The coefficient of each new basis vector is a polynomial function. The basic idea for the improvement of the solution

is to replace these polynomials by rational functions (ratio of two polynomials) called Padé approximants. An updated representation of this subject can be found in the book of Baker and Graves-Morris [48]. This technique is largely tested to extend the domain of convergence of the polynomial representation [38, 40]. Recall that the kernel of the operator $\mathbf{L}$ is assumed to be one-dimensional and generated by the vector $\mathbf{U}_1$. The vectors $\mathbf{U}_p$ are orthogonal to $\mathbf{U}_1$ but not with each other. To obtain an orthogonal basis, use the classical Gram-Schmidt orthogonalization procedure. The new orthogonal basis is defined by:

$$\begin{cases} \mathbf{U}_1^{\perp} = \mathbf{U}_1, \\ \\ \mathbf{U}_p^{\perp} = \mathbf{U}_p - \sum_{j=1}^{p-1} \alpha_{p,j} \mathbf{U}_j^{\perp}, \end{cases} \tag{39}$$

where the coefficients $\alpha_{p,j}$ can be numerically computed by the following formulae

$$\alpha_{p,j} = \frac{\langle \mathbf{U}_p, \mathbf{U}_j^{\perp} \rangle}{\langle \mathbf{U}_j^{\perp}, \mathbf{U}_j^{\perp} \rangle}. \tag{40}$$

Insertion of equations (39) into equation (17a) leads to a new representation of the solution $\mathbf{U}(a)$ given by:

$$\begin{aligned} \mathbf{U}(a) = {} & a\mathbf{U}_1^{\perp} \\ & + a^2\mathbf{U}_2^{\perp}\left[1 + \sum_{k \geqslant 1} a^2 \alpha_{k+2,2}\right] \\ & + \ldots \\ & + a^p\mathbf{U}_p^{\perp}\left[1 + \sum_{k \geqslant 1} a^k \alpha_{k+p,p}\right] + \ldots . \end{aligned} \tag{41}$$

The series

$$\left(1 + \sum_{k \geqslant 1} a^k \alpha_{k+j,j}\right)$$

can be approximated by the Padé approximant $P_j[L_j, M_j](a)$, which is a rational fraction given by:

$$P_j[L_j/M_j](a) = \left(\frac{b_0^j + b_1^j a + \cdots + b_{Lj}^j a^{Lj}}{1 + c_1^j a + \cdots + c_{Mj}^j a^{Mj}}\right), \tag{42}$$

where L_j and M_j are the degrees of the polynomial fraction of denominator and numerator respectively. This rational function is defined such as its Maclaurin expansion agrees with the power series through order $L_j + M_j$.

$$1 + \sum_{k \geqslant 1} a^k \alpha_{k+j,j} = P_j[L_j, M_j](a) + O(a^{L_j + M_{j+1}}) \tag{43}$$

The $M_j + L_j + 1$ coefficients b_i^j and c_i^j for each j can be computed by solving a linear system [48]. Thus, a rational function representation of the solution $U(a)$ is defined by

$$U(a) = \sum_{j=1}^{\infty} a^j P_j[L_j, M_j](a) U_j^{\perp}. \tag{44}$$

The representation of the frequency parameter can be easily obtained from (16a) as follows:

$$\omega^2(a) - \omega_L^2 = \frac{\langle \mathbf{Q}(\mathbf{U}(a), \mathbf{U}(a)); \mathbf{U}_1 \rangle}{\langle \mathbf{M} \cdot \mathbf{U}(a); \mathbf{U}_1 \rangle} \tag{45}$$

Finally, the solution of the problem (16a) is giving by the rational representations (44, 45). Now recall that the manipulation and computation of the vectors $\mathbf{U}_p^{\perp}$ and the Padé approximants $P_j[L_j, M_j]$ require little computation time. Only the orders L_j and M_j of each Padé approximant (42) have to be chosen [38, 40]. This leads to the construction of a sequence of these approximants. It is expected that a well-chosen sequence will normally increase the zone of validity of the solution. The major difficulty in applying this technique is the choice of those orders. Nevertheless, there is no rigorous justification of the convergence of these approximants. An empirical convergence is regarded as entirely satisfactory within its limitations. A criterion which has worked well here is the choice of $P[L, M]$ such that ($M - L = 2$ or $M - L = 1$). Some details of these constructions for a given order are presented in Appendix B. In order to limit the number of poles of these Padé approximants and to increase the robustness of this algorithm a new way to build up these approximants has been presented [49].

4.3. ABOUT COMPUTATIONAL COST

For computational effort, these methods have been successfully tested in various studies. The computational cost of these methods have been compared with other numerical methods in some published results [39, 42, 49–52]. For a problem of 2000 to 5000 d.o.f., the computation of the series at orders 20 necessitates 50% of additional computational time with respect to linear calculation. For this reason, the methods presented here are more effective than the Newton–Raphson algorithm, especially for bifurcating branches, in which case it is difficult to define an efficient computational strategy [51].

As for the reduced basis technique [22], a detailed comparison has been done in reference [49]. As expected, the later method yields greater ranges of validity than the representation by series and by Padé approximants, but the difference is not so large, especially with Padé approximants. In contrast, the reduced basis technique should be used only with small orders of truncation, since the time to get the reduced system increases rapidly when this order increases. Clearly, the two methods presented here with a large order of truncature (15 to 25) lead to greater step lengths than the reduced basis technique at a small order (7 to 10), with similar computational cost, see reference [49]. That is why reference [49] recommends the representation by Padé approximants, "so long as a cheap algorithm to compute

the coefficients of the reduced problem has not been found". Recently, a robust continuation method based on that rational representation has been established [52].

5. NUMERICAL RESULTS

There are many parameters that can be varied in non-linear vibration of plates so that it would be difficult to present and compare results of all cases. Only a few typical cases will be selected for discussion. To illustrate the effectiveness of this method, comprehensive numerical tests are investigated. The validity of the obtained results is demonstrated by comparing them with those available in the literature. For large amplitude vibrations, the continuation method and Padé approximants are clearly presented and applied for various shapes and boundary conditions of plates. The backbone curves of fully clamped square and circular plates are presented in Figures 1 and 2. It is clearly shown that results predicted by this method agree well with those reported in the literature. Part of the backbone curve is obtained analytically in one step needing numerical solution of linear problems having the same matrix. The validity of the predicted results is limited by the radius of convergence of the series (29). Taking the starting point in the zone of validity and reapplying the asymptotic numerical method, one obtains a path following method giving analytically the whole of the backbone curve. In Figure 3, is presented the large amplitude frequency curves for a simply supported and a fully clamped circular plate by iterating the ANM. The symbol (-◇-) indicates the starting point of the method. For a simply supported case, one obtains the resonant curve up to $\omega = 4\omega_L$ in two steps and for a fully clamped case the same result is obtained in three steps. The solution is obtained by iterating

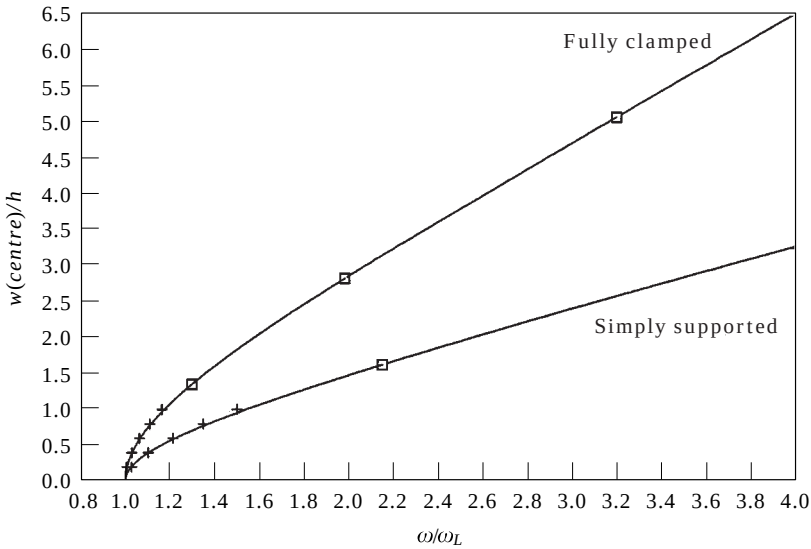

Figure 3. Displacement–frequency curve for a simply supported and fully clamped isotropic circular plate by the iterating ANM. □ indicates the starting point of the ANM and (+) indicates the results of reference [15].

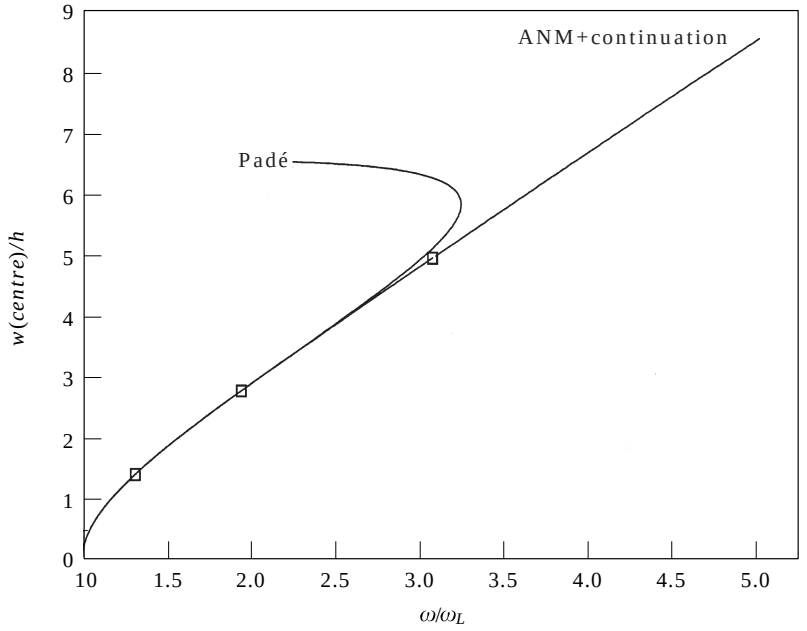

Figure 4. Displacement–frequency curve for a fully clamped square plate by iterating Asymptotic-Numerical Method and by Padé approximants. □ indicates the starting point of the ANM.

the ANM and compared with Reddy *et al*.'s results [15] obtained by FEM and an iterating eigenvalue technique. Comparison between Figures 2 and 3 in the fully clamped case shows clearly that the limitation of the solution obtained has been overcome and the totality of the backbone curve can be derived. This clearly shows the effectiveness of the method in order to obtain a large part of the non-linear branch in a few steps.

The use of the Padé approximants procedure permits one to rearrange the series (29) in order to extract from them the maximum amount of information. This shrewd process permits one increase considerably the zone of validity without more computation time. The effectiveness and reliability of these procedures are clearly presented in the Figures 4 and 5. In these figures are presented the transverse displacement at the centre versus the frequency ratio of a fully clamped isotropic square and rectangular plate by iterating the ANM and by Padé approximants. It is apparent that the limitation of the validity of the solution presented in Figure 1 has been overcome and the prolongation of the backbone curve is determined. Then, the large amplitude solution is easily computed for a desired range. The presented part of the solution is obtained in four steps. The use of Padé approximants presented above permitted a threefold increase in the zone of validity of the solution before diverging. The greatest advantage of this procedure is that a simple rearrangement of the series (29) and a good choice of the approximants permits one to obtain a very large part of the solution. Obviously, the major difficulty in applying this procedure is how to direct the choice in order to obtain the best approximants. A solution of Paolé approximants having singularity points out of the desired zone is usually used. For an automatic

computation, a criterion for the choice depending on the shape of the solution is needed. The criterion used here is presented in Appendix B.

As presented in Tables 1 and 2, the results obtained by this method agree well with those obtained by the assumed one-mode analysis, especially for the simply supported case. The one-dimensional analysis gives good predictions for the non-linear frequency against the amplitude at the centre of the plate but leads to erroneous results for the displacement which remains proportional to the first mode. In Figure 6, is presented the linear and non-linear modes for simply supported boundary conditions at the centre and at the quarter of a square plate for various amplitudes. In this case there is a small discrepancy between linear and non-linear modes. In Figures 7 and 8, are presented linear and non-linear modes at various amplitudes for fully clamped square and rectangular plates, respectively. In these cases, one can clearly see that there is a wide discrepancy between the linear and non-linear modes. This illustrates the limitation of the one-mode analysis which leads to erroneous results for the non-linear mode at large amplitudes. In Figures 9 and 10, are presented the first three and two backbone curves for square and rectangular plates, respectively. All these results are obtained in three steps of the ANM. In Figure 11, is presented the backbone curve of a fully simply supported annular plate obtained by the two procedures, where ($R1 = 1$) is the internal radius of the hole and ($R2 = 10$) is the external radius of the circular plate. In this case, the zone of validity of the series (29) is very small ($w(R2 - R1)/2$, $(R2 - R1)/2) = 0{\cdot}4h$). Four iterations of the ANM give the solution until ($\omega = 3{\cdot}4\omega_L$). The Padé approximant solution obtained by the same criterion as in Figures 4 and 5 coincides with the ANM solution except at the

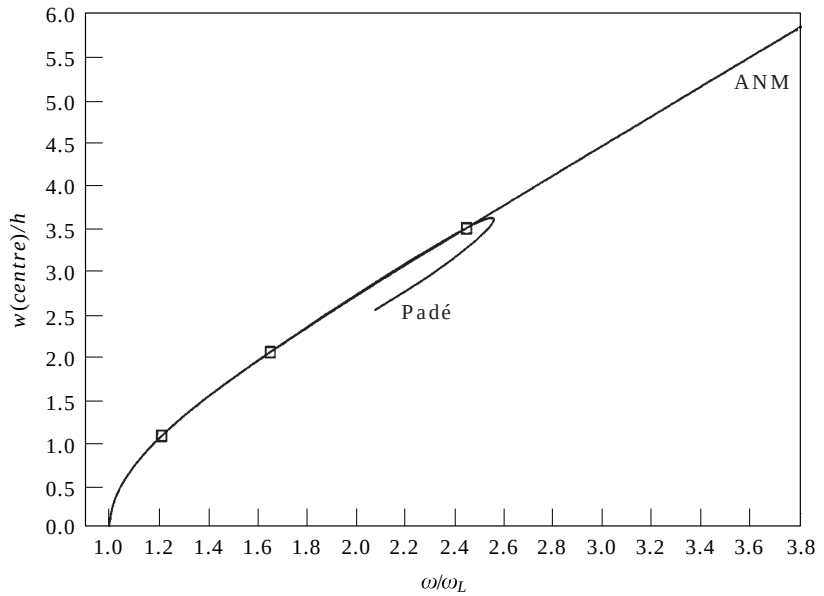

Figure 5. Displacement–frequency curve for a fully clamped rectangular plate (length/width = 2) by iterating Asymptotic-Numerical Method and by Padé approximants. □ indicates the starting point of the ANM.

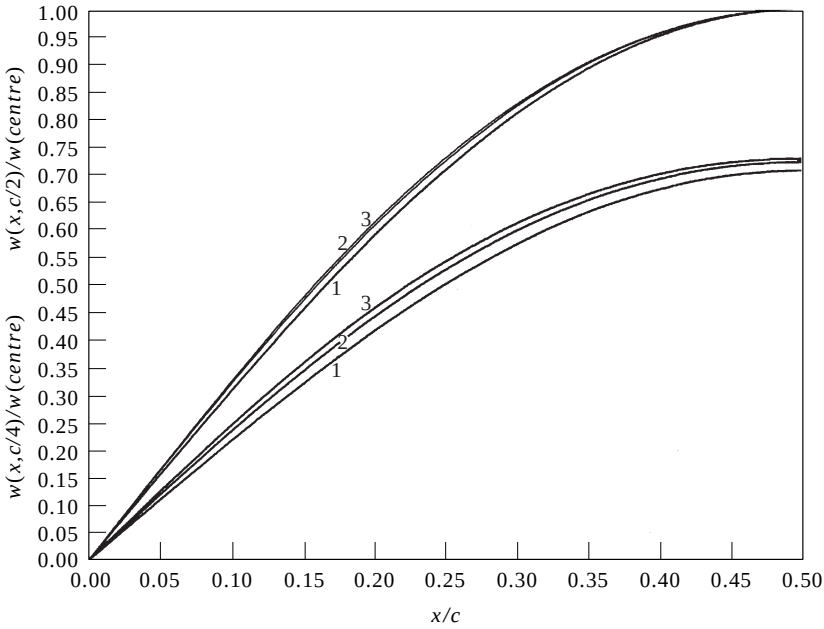

Figure 6. Linear and non-linear mode shapes at the centre and at the quarter of a simply supported square plate at various amplitudes. c is the side of the plate and $w(centre) = w(c/2, c/2)$. 1: linear mode, 2: non-linear mode at $w(centre) = 2{\cdot}0018h$, and 3: non-linear mode at $w(centre) = 3{\cdot}5039h$.

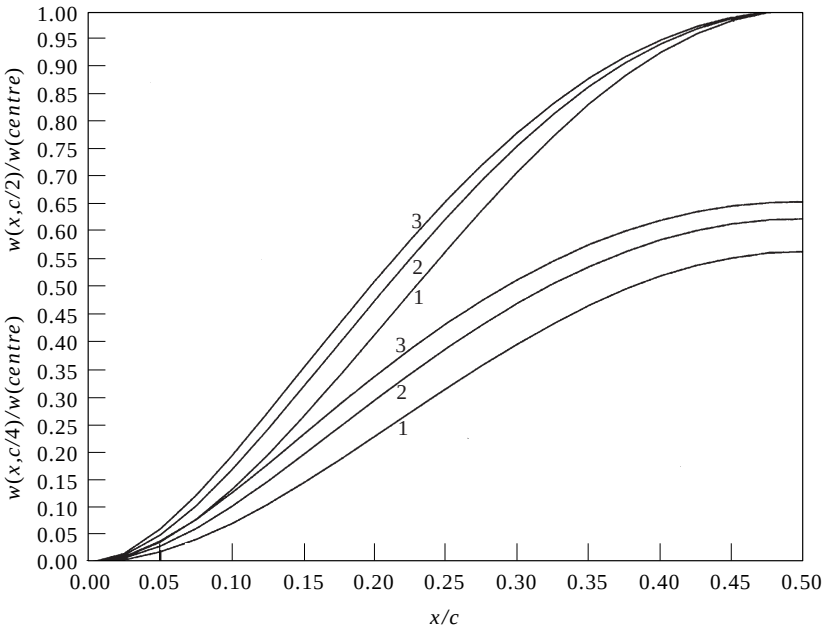

Figure 7. Linear and non-linear mode shapes at the centre and at the quarter of a fully clamped square plate at various amplitudes. c is the side of the plate and $w(centre) = w(c/2, c/2)$. 1: linear mode, 2: non-linear mode at $w(centre) = 2{\cdot}005h$, and 3: non-linear mode at $w(centre) = 3{\cdot}006h$.

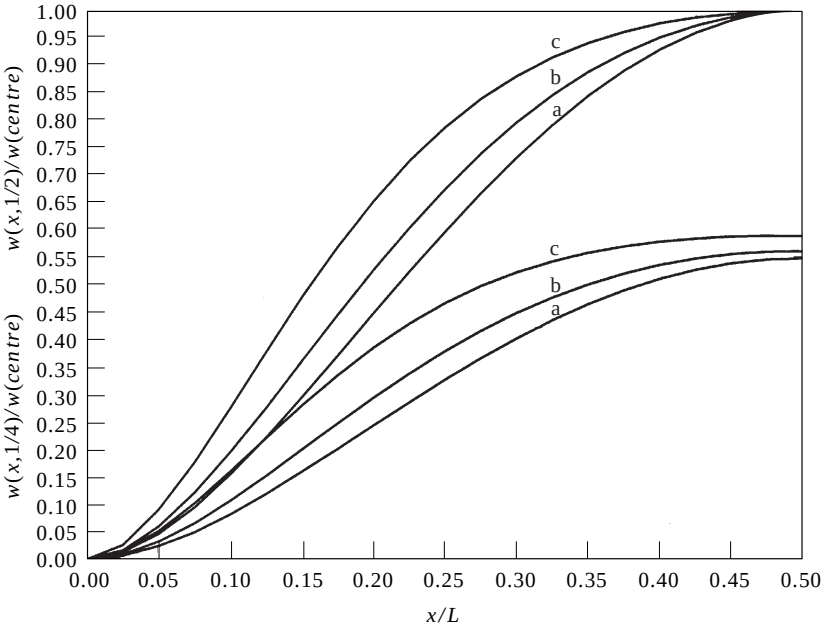

Figure 8. Linear and non-linear mode shapes at the centre and at the quarter of a fully clamped rectangular plate at various amplitudes. L is the length and l is the width of the plate ($L/l = 2$), $w(centre) = w(L/2, l/2)$. a: linear mode, b: non-linear mode at $w(centre) = 1{\cdot}0005h$, and c: non-linear mode at $w(centre) = 2{\cdot}0057h$.

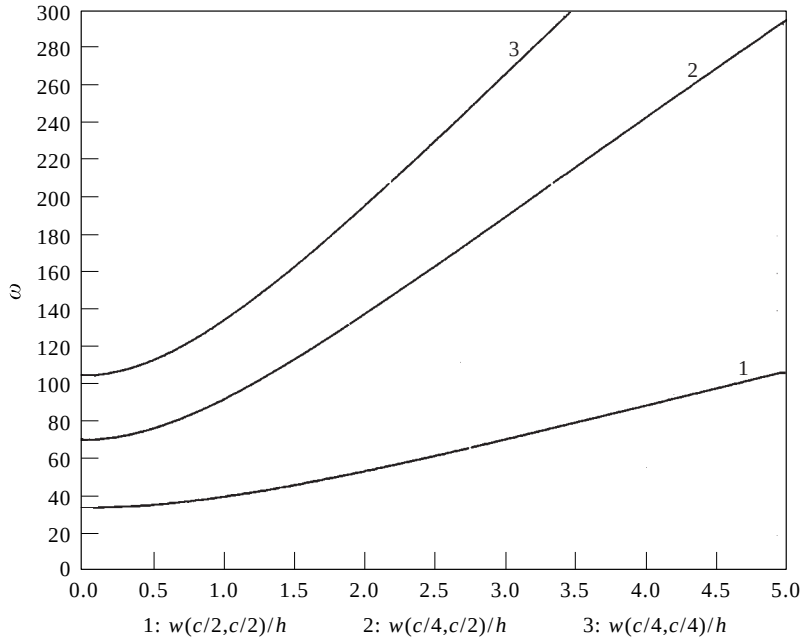

Figure 9. The first three backbone curves for a fully clamped square plate obtained by three iterations of the ANM.

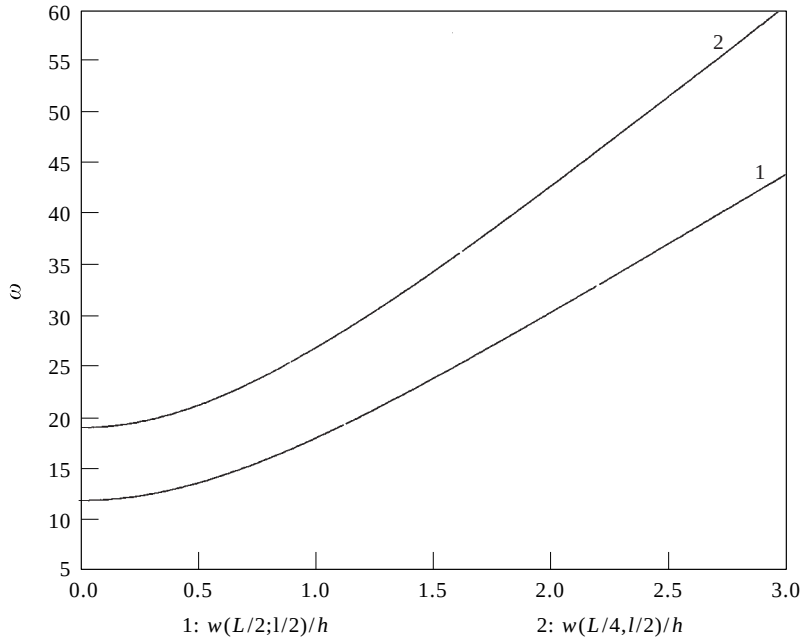

Figure 10. The first two backbone curves for a simply supported rectangular plate, (length/width = 2) obtained by three iterations of the ANM.

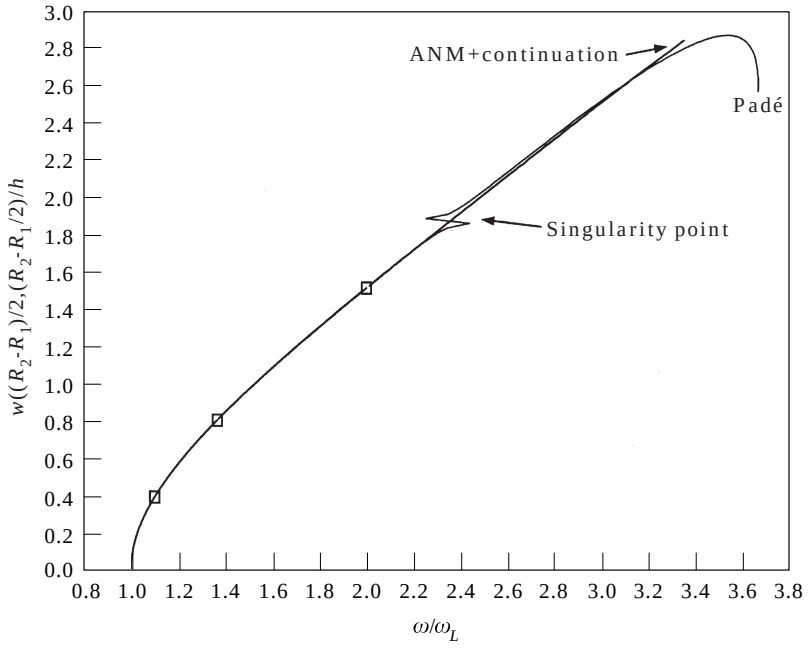

Figure 11. Displacement–frequency curve for a simply supported annular plate by iterating Asymptotic-Numerical Method and by Padé approximants. □ indicates the starting point of the ANM. $R_1 = 1$ is the interior radius and $R_2 = 10$ is the external one.

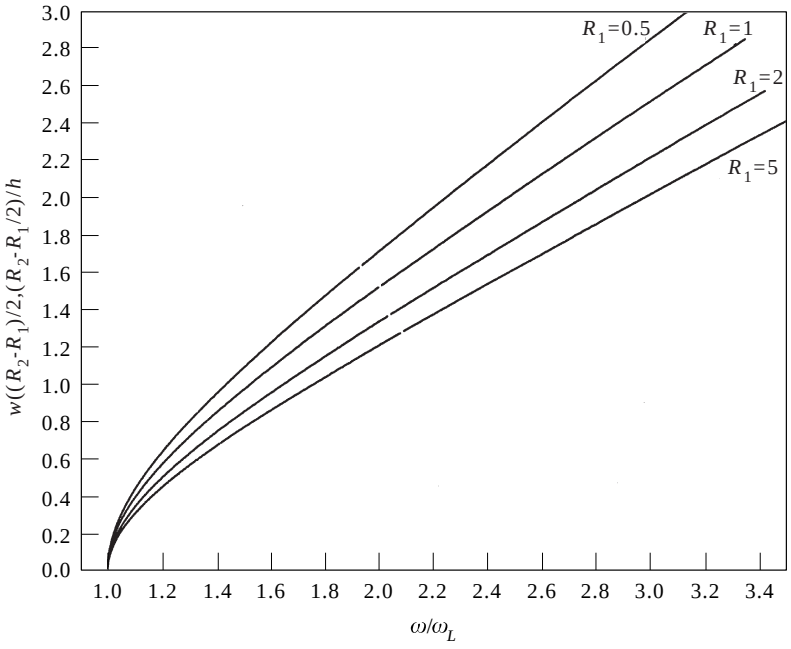

Figure 12. Displacement–frequency curve for fully simply supported annular circular plates with various internal radii. $R_2 = 10$ is the external radius and $R_1 = 0{\cdot}5$, 1, 2, 5 is the radius of the circular hole, $R_2/h = 100$.

singular point. These figures clearly show that this amazing technique greatly increases the solution obtained by the asymptotic series (29) without more computation time. In Figure 12, is presented the backbone curve of a simply supported annular circular plate with variation of the radius of the hole. The results are obtained by three steps of the ANM. Finally, the method presented is an effective tool capable of tracing the whole of the backbone curve in a few steps with little computation time. This effectiveness will be very fruitful in studing more complicated structural vibrations or internal resonance appearing when one takes into account more terms of the time series.

6. CONCLUSION

The applicability of the Asymptotic-Numerical Method to study the large amplitude vibrations of plates with various geometries and boundary conditions has been demonstrated. Based on the von Karman model and on the harmonic balance method, the dynamic problem of plate vibration is transformed into a static one. A non-linear operational formulation has been obtained. The Asymptotic-Numerical Method based on the finite element method has been applied for the solution. The principle of this method is to compute numerically some series that give the displacement, the stress and the frequency as a function of a perturbation parameter. In order to simplify the expansion procedure, a mixed formulation of the governing equation has been used which leads to a quadratic non-linearity. Hence, a very large number of terms of the series can be easily

computed. Numerical results for non-linear frequency and non-linear displacement are presented and compared. Presented results agree well with the results available in the literature. For large amplitude vibrations, the iterating ANM and Padé approximants procedures are incorporated. The backbone curves are successfully obtained for different shapes and boundary conditions of the plate at very large amplitudes.

The main advantages of this method are as follows:

In comparison with classical perturbation methods, a great number of terms of the perturbed series can be easily and automatically computed. The Padé approximants procedure for improving the range of validity of the solution can be easily added without more computation time.

A path following technique via the iteration of ANM with analytical large steps is successfully used. In comparison with traditional step by step procedures, the present method has the following advantages: it is simple and computationally efficient. Indeed, the expansion technique transforms the non-linear problem into a sequence of linear ones with a single stiffness matrix. Hence, the computation time is of the same order as for a single step of the modified Newton–Raphson algorithm; the backbone curve is known continuously and not only at some points; the computation of the series is fully automatic. The only parameters that have to be chosen are the order of truncature, the small parameter ε to define a new starting point and the number of the desired iterations; the range of validity of the step length is given by the method itself and it is not chosen *a priori* by the user.

In summary, this method is efficient and reliable. It has been illustrated here for large amplitude vibrations of plates with different shapes and boundary conditions. Other related topics, such as forced non-linear vibrations, internal resonance and non-linear damped vibrations of thin elastic structures, may be investigated later using the techniques developed here.

REFERENCES

1. N. Yamaki 1961 *Zeitschrift fur Angewandte Mathematik and Mechanik* **41**, 501–510. Influence of large amplitudes on flexural vibrations of elastic plates.
2. T. Wah and M. Asce 1963 *Journal of Engineering Mechanics Division*, *ASCE* **89**(EM5), 1–15. Vibration of circular plates at large amplitudes.
3. J. G. Eisley 1964 *Zeitschrift fur Angewandte Mathematik and Physik* **15**, 167–175. Nonlinear vibration of beams and rectangular plates.
4. A. V. Srinivasan 1966 *International Journal of Nonlinear Mechanics* **1**, 179–191. Nonlinear vibrations of beams and plates.
5. B. Nageswara Rao and S.R.R. Pillai 1992 *Journal of Sound and Vibration* **154**, 173–177. Large amplitude free vibrations of laminated anisotropic thin plates based on harmonic balance method.
6. B. Nageswara Rao and S. R. R. Pillai 1992 *Journal of Sound and Vibration* **152**, 568–572. Nonlinear vibrations of a simply supported rectangular anti-symmetric cross-ply plate with immovable edges.
7. S. R. R. Pillai and B. Nageswara Rao 1993 *Journal of Sound and Vibration* **160**, 1–6. Reinvestigation of nonlinear vibrations of simply supported rectangular cross-ply plates.

8. G. Singh, K. Kanaka Raju and G. Venkateswara Rao 1990 *Journal of Sound and Vibration* **142**, 213–226. Nonlinear vibrations of simply supported rectangular cross-ply plates.
9. J. Woo and S. Nair 1992 *American Institute of Aeronautics and Astronautics Journal* **30**, 180–188. Nonlinear vibrations of rectangular laminated thin plates.
10. M. Sathyamoorthy 1983 *Shock and Vibration Digest* **15**, 3–16. Nonlinear vibrations of plates, a review
11. C. Y. Chia 1980 *Nonlinear analysis of plates*. New York: McGraw-Hill.
12. I. S. Raju, G. Venkateswara Rao and K. Kanaka Raju 1976 *Journal of Sound and Vibration* **49**, 415–422. Effect of longitudinal or in-plane deformation and inertia on the large amplitude flexural vibrations of slender beams and thin plates.
13. C. Mei 1973 *Computers and Structures* **3**, 163–174. Finite element displacement method for large amplitude free flexural vibrations of beams and plates.
14. G. Venkateswara Rao, K. Kanaka Raju and I. S. Raju 1976 *Computer and Structures* **6**, 169–172. Finite element formulation for the large amplitude free vibrations of beams and orthotropic circular plates.
15. J. N. Reddy and C. L. Huang 1981 *Journal of Sound and Vibration* **79**, 387–396. Large amplitude free vibrations of annular plates of varying thickness.
16. J. N. Reddy, C. L. Huang and I. R. Singh 1981 *International Journal for Numerical Methods in Engineering* **17**, 527–541. Large deflections and large amplitude vibrations of axisymmetric circular plates.
17. C. Mei and Kamolphan Decha-Umphai 1985 *American Institute of Aeronautics and Astronautics Journal* **23**, 1104–1110. A finite element method for nonlinear forced vibrations of rectangular plates.
18. T. Kant and J. R. Kommineni 1994 *Computer and Structures* **50**, 123–134. Large amplitude free vibration analysis of cross-ply composite and sandwich laminates with a refined theory and C° finite elements.
19. P. C. Dumir and A. Bhaskar 1988 *Journal of Sound and Vibration* **123**, 517–527. Some erroneous finite element formulations of nonlinear vibrations of beams and plates.
20. L. Carter Wellford Jr., G. M. Dib and W. Mindle 1890 *Earthquake Engineering and Structural Dynamics* **8**, 97–115. Free and steady state vibration of nonlinear structures using finite element nonlinear eigenvalue technique.
21. S. L. Lau, Y. K. Cheung and S. Y. Wu 1984 *Journal of Applied Mechanics* **51**, 837–844. Nonlinear vibration of thin elastic plates. Part I: Generalised incremental Hamilton's principle and finite element formulation.
22. A. K. Noor, C. M. Andersen and J. M. Peters 1993 *Computational Method in Applied Mechanics and Engineering* **103**, 175–186. Reduced basis technique for nonlinear vibration analysis of composite panels.
23. R. Lewandowski 1987 *Journal of Sound and Vibration* **114**, 91–101. Application of the Ritz method to the analysis of nonlinear free vibrations of beams.
24. R. G. White and C. E. Teh 1981 *Journal of Sound and Vibration* **75**, 527–547. Dynamic behaviour of isotropic plates under combined acoustic excitation and static in-plane compression.
25. R. Benamar 1990 *Ph.D. Thesis*, *University of Southampton*. Nonlinear dynamic behaviour of fully clamped beams and rectangular isotropic and laminated plates.
26. R. Benamar, M. M. K. Bennouna and R. G. White 1993 *Journal of Sound and Vibration* **164**, 399–424. The effects of large vibration amplitudes on the mode shapes and natural frequencies of thin elastic structures. Part II: fully clamped rectangular plates.
27. R. Benamar, M. M. K. Bennouna and R. G. White 1994 *Journal of Sound and Vibration* **175**, 377–395. The effects of large vibration amplitudes on the mode shapes and natural frequencies of thin elastic structures. Part III: Fully clamped rectangular isotropic plates-measurements of the mode shape amplitude dependence and the spatial distribution of harmonic distortion.

28. L. Azrar and R. Benamar 1995 *5ème Colloques Maghrébin sur les Modèles Numériques de l'Ingénieur*, *E.M.I.*, *Rabat*, *Maroc*, 594–599. Etude des vibrations non linéaires forcées des poutres par une méthode semi-analytique.
29. L. Azrar, R. Benamar and R. G. White 1998 *Journal of Sound and Vibration* (in press). A semi analytical approach to the nonlinear dynamic response problem of S-S and C-C beams at large vibration amplitudes. Part I: general theory and application to the single mode approach to free and forced vibration analysis.
30. A. H. Nayfeh 1973 Perturbation methods. New York: John Wiley and Sons.
31. S. Sridhar, D. T. Mook and A. H. Nayfeh 1975 *Journal of Sound and Vibration* **41**, 359–373. Nonlinear resonances in the forced responses of plates. Part I: Symmetric response of circular plates.
32. A. H. Nayfeh and S. A. Nayfeh 1994 *Journal of Vibration and Acoustics* **116**, 129–136. On nonlinear modes of continuous systems.
33. Y. K. Cheung and S. L. Lau 1982 *Earthquake Engineering and Structural Dynamics* **10**, 239–253. Incremental time-space finite strip method for nonlinear structural vibrations.
34. A. Aprile, A. Benedetti and T. Trombetti 1994 *Earthquake Engineering and Structural Dynamics* **23**, 363–388. On nonlinear dynamic analysis in the frequency domain: algorithms and applications.
35. N. Damil and M. Potier-Ferry 1990 *International Journal of Engineering and Sciences* **28**, 943–957. A new method to compute perturbed bifurcation: application to the buckling of imperfect elastic structures.
36. L. Azrar, B. Cochelin, N. Damil and M. Potier-Ferry 1992 in *New Advances in computational structural mechanics* (P. Ladevèze and O. C. Zienkiewicz, editors) 117–131. Amsterdam: Elsevier Science. An Asymptotic Numerical Method to compute bifurcating branches.
37. L. Azrar and M. Potier-Ferry 1992 *Numerical Methods in Engineering* (Ch. Hirsch *et al*., editors) 607–614. Amsterdam: Elsevier Science. Post-buckling of imperfect structures by an Asymptotic- Numerical Method.
38. L. Azrar 1993 *Thèse de Doctorat de l'Université de Metz*, *France*. Etude du comportement post- critique des coques cylindriques par une Méthode Asymptotique Numérique.
39. L. Azrar, B. Cochelin, N. Damil and M. Potier-Ferry 1993 *International Journal for Numerical Methods in Engineering* **36**, 1251–1277. An Asymptotic Numerical Method to compute the post-buckling behaviour of elastic plates and shells.
40. B. Cochelin, N. Damil and M. Potier-Ferry 1994 *International Journal for Numerical Methods in Engineering* **37**, 1187–1213. Asymptotic-Numerical Method and Padé approximants for nonlinear elastic structures.
41. B. Cochelin 1994 Computer and Structures **53**, 1181–1192. A path-following technique via an Asymptotic-Numerical Method.
42. L. Azrar, B. Cochelin, N. Damil and M. Potier-Ferry 1998 *Structural Dynamic Systems* **7**, (Gordon & Breach series in press). An Asymptotic-Numerical Method for nonlinear vibrations of elastic structures.
43. O. C. Zienkiewicz 1977 *The finite element method*. London: McGraw-Hill; 3rd edition.
44. J. L. Batoz, K. J. Bathe and L. W. Ho 1980 *International Journal for Numerical Methods in Engineering* **15**, 1771–1812. A study of three node triangular plate bending elements.
45. M. A. Crisfield 1983 *International Journal for Numerical Methods and Engineering* **19**, 1269–1289. An arc-length method including line search and acceleration.
46. E. Riks 1984 *Computer Methods in Applied Mechanics and Engineering* **47**, 219–259. Some computational aspects of the stability analysis of nonlinear structures.
47. E. Carrera 1994 *Computer and Structures* **50**, 217–229. A study on arc-length-type methods and their operation failures illustrated by a simple model.

48. G. A. Baker and P. Graves-Morris 1981 *Encyclopaedia of Mathematics and its applications*, Volume 13. Padé approximants, Part I: basic theory. Reading, MA: Addison-Wesley.
49. A. Najah, B. Cochelin, N. Damil and M. Potier-Ferry 1998 *Archives of Computational Methods in Engineering* **5**, 3–22. A critical review of asymptotic numerical methods.
50. J. M. Cadou 1997 *Thèse de Doctorat de l'Université de Metz, France*. Méthode asymptotique numérique pour le calcul des branches de solutions et des instabilités dans les fluides et pour les instabilités d'interaction fluide-structure.
51. H. Zahrouni 1998 *Thèse de Doctorat de l'Université de Metz, France*. Méthode asymptotique numérique pour les coques en grandes rotations.
52. A. Elhage-Hussein, N. Damil and M. Potier-Ferry 1998 *Revue Européenne des Eléments Finis* **7**, 119–130. An asymptotic numerical algorithm for frictionless contact problems.

APPENDIX A

The aim of this appendix is to present the right hand side of equations (20) and (23). At order p, one has to solve the following problem:

$$\begin{cases} \langle \mathbf{L} \cdot \mathbf{U}_p; \delta\mathbf{U} \rangle = \langle \mathbf{F}_p; \delta\mathbf{U} \rangle, \\ \langle \mathbf{U}_p; \mathbf{U}_1 \rangle = 0, p > 1. \end{cases}$$

The operator $\langle \mathbf{L} \cdot (\,); \delta\mathbf{U} \rangle$ is defined by equation (16b) and the right-hand side is given by:

$$\langle \mathbf{F}_p; \delta\mathbf{U} \rangle = \int_\Omega \{ \mathbf{F}^U p \delta\mathbf{U} + \tfrac{3}{4}\mathbf{F}^w_\alpha(p)\delta w_{,\alpha} + \tfrac{3}{4}\mathbf{F}^N_{\alpha\beta}(p)\delta N_{\alpha\beta} \}\, \mathrm{d}\Omega$$

where $\mathbf{F}^U$, F^w_α and $F^N_{\alpha\beta}$ are given by:

$$\mathbf{F}^U(p)\delta\bar{\mathbf{U}} = \rho h \sum_{r=1}^{p-1} C(r)[u(p-r)\delta u + v(p-r)\delta v + w(p-r)\delta w],$$

$$\mathbf{F}^w_\alpha(p) = -\sum_{r=1}^{p-1} N_{\alpha\beta}(r) w_{,\beta}(p-r),$$

$$\mathbf{F}^N_{\alpha\beta}(p) = -\sum_{r=1}^{p-1} \tfrac{1}{2} w_{,\alpha}(r) w_{,\beta}(p-r).$$

APPENDIX B

In this appendix, some details are given about the construction of Padé approximants and the strategy followed for numerical results presented in Figures 4, 5 and 11. Let us consider the case of truncation of the series at the order $n = 20$.

By the ANM, one obtains the vectors $\mathbf{U}_1, \mathbf{U}_2, \ldots \mathbf{U}_{20}$ and the solution $\mathbf{U}(a)$ is given by:

$$\mathbf{U}(a) = a\mathbf{U}_1 + a^2\mathbf{U}_2 + \cdots + a^{20}\mathbf{U}_{20}. \tag{B1}$$

Using the Gram-Schmidt orthogonalization procedure, one can easily obtain

$$\begin{cases} \mathbf{U}_1 = \mathbf{U}_1^{\perp} \\ \mathbf{U}_p = \mathbf{U}_p^{\perp} + \sum_{j=1}^{p-1} \alpha_{p,j}\mathbf{U}_j^{\perp}; \quad \alpha_{p,j} = \dfrac{\langle \mathbf{U}_p, \mathbf{U}_j^{\perp} \rangle}{\langle \mathbf{U}_j^{\perp}, \mathbf{U}_j^{\perp} \rangle}, \end{cases} \tag{B2}$$

$\alpha_{p,1} = 0$, because of the orthogonality condition $\langle \mathbf{U}_1, \mathbf{U}_p \rangle = 0$ for $p > 1$.

The insertion of (B2) into (B1) leads to:

$$\mathbf{U}(a) = a\mathbf{U}_1^{\perp} + a^2\mathbf{U}_2^{\perp}\left[1 + \sum_{k=1}^{18} a^k\alpha_{k+2,2}\right] + a^3\mathbf{U}_3^{\perp}\left[1 + \sum_{k=1}^{17} a^k\alpha_{k+3,3}\right] + \ldots$$

$$+ a^{12}\mathbf{U}_{12}^{\perp}\left[1 + \sum_{k=1}^{8} a^k\alpha_{k+12,12}\right] + \ldots$$

$$\mathbf{U}(a) = a\mathbf{U}_1^{\perp} + a^2\mathbf{U}_2^{\perp}P_2[\mathbf{L}_2, \mathbf{M}_2](a) + a^3\mathbf{U}_3^{\perp}P_3[L_3, M_3](a)$$
$$+ a^4\mathbf{U}_4^{\perp}P_4[L_4, M_4](a) + \cdots + a^{12}\mathbf{U}_{12}^{\perp}P_{12}[L_{12}, M_{12}](a)] + \ldots \tag{B3}$$

where $P_j[L_j, M_j](a)$ approximates the series

$$\left(1 + \sum_{k=1}^{n-j} a^k\alpha_{k+j,j}\right).$$

The construction of these approximants necessitates a numerical solution of two linear systems given the $(L_j + M_j + 1)$ coefficients of the numerator and the denominator of $P_j[L_j, M_j](a)$ [38, 40, 48, 49]. It is common practice to display the approximants in a table, called a Padé table, and to choose the best ones that have singularity outside the desired zone. A criterion which was used for numerical solutions presented in these studies is the choice of $P[L, M](a)$ such that $M - L = 2$ or $M - L = 1$ and truncated at order 12.

$$\mathbf{U}(a) = a\mathbf{U}_1^{\perp} + a^2\mathbf{U}_2^{\perp}P[8, 10](a) + a^3\mathbf{U}_3^{\perp}P[8, 9](a) + a^4\mathbf{U}_4^{\perp}P[7, 9](a)$$
$$+ a^5\mathbf{U}_5^{\perp}P[7, 8](a)$$
$$+ a^6\mathbf{U}_6^{\perp}P[6, 8](a) + a^7\mathbf{U}_7^{\perp}P[6, 7](a) + a^8\mathbf{U}_8^{\perp}P[5, 7](a) + a^9\mathbf{U}_9^{\perp}P[5, 6](a)$$
$$+ a^{10}\mathbf{U}_{10}^{\perp}P[4, 6](a) + a^{11}\mathbf{U}_{11}^{\perp}P[4, 5](a) + a^{12}\mathbf{U}_{12}^{\perp}P_{12}[3, 5](a).$$

Obviously, a selection of the Padé approximants in (B3), that have singularities outside of the desired zone, can lead to more accurate results than those presented here.

APPENDIX C: NOTATION

x, y, z	Cartesian co-ordinates
t	time variable
u, v, w	displacement components in x, y and z directions, respectively
$\mathbf{\Gamma}^L, \mathbf{\Gamma}^{NL}$	linear and non-linear parts of the strain tensor
$\boldsymbol{\gamma}^L, \boldsymbol{\gamma}^{NL}$	linear and non-linear parts of the strain tensor without time
$\boldsymbol{\kappa}$	bending strain tensor
$\mathbf{N}, \mathbf{M}$	in-plane stress and moment resultants
h, ρ	thickness and mass density
E, v	Young's modulus and Poisson's ratio
P	potential energy
T	kinetic energy
$\mathbf{U} = [u, v, w, \mathbf{N}]$	mixed displacement–stress vector field
H	mixed functional
ω_L, ω	linear and non-linear frequencies
$[\mathbf{C}_m], [\mathbf{C}_b]$	membrane and bending matrices
$\mathbf{L}$	stiffness linear operator
$\mathbf{M}$	mass operator
$\mathbf{Q}$	non-linear operator
$\mathbf{U}_p = [u_p, v_p, w_p, \mathbf{N}_p]$	mixed vector field at order p of the power series expansions of the vector $\mathbf{U}$
$C_{(p)}$	coefficient at order p of the power series expansion of the frequency ω
$\bar{\mathbf{U}} = [u, v, w]$	pure displacement vector
$\bar{\mathbf{L}}$	pure displacement stiffness operator
$\bar{\mathbf{F}}_{(p)}$	right hand side at order p
$[\mathbf{K}e], [\mathbf{M}]$	stiffness and mass matrices
$[\mathbf{K}t]$	tangent matrix
$\mathbf{U}_0$	starting point for the continuation process
$\mathbf{L}_t$	tangent operator
$\mathbf{V}_p$	displacement vector at order p of the power series expansions of the displacement around the starting point $\mathbf{U}_0$
s	scaling parameter
$\mathbf{U}_j^{\perp}$	vector fields after orthogonalisation
$P_j[L_j, M_j]$	Padé approximant